UNIVERSITY OF CALIFORNIA SAN DIEGO

Unraveling RNA-Binding Protein Mislocalization in Neurodegenerative Disorders

A Dissertation submitted in partial satisfaction of the requirements
for the degree Doctor of Philosophy

in

Neuroscience

by

Norah Al-Azzam

Committee in charge:

Professor Gene Yeo, Chair
Professor Ludmil Alexandrov
Professor Nicole Coufal
Professor John Ravits

2024

The Dissertation of Norah Al-Azzam is approved, and it is acceptable in quality and form for publication on microfilm and electronically.

University of California San Diego

2024

DEDICATION

Throughout my journey, I have relied heavily on my family. They provide me with strength when I am weak, happiness when I am sad, and life when I don't feel like living. I would not have been able to achieve all my success without my beloved mother, Mayada Rasheed; my caring and humorous father, Ali Al-Azzam; my twin brother who drives me crazy, Mustafa Al-Azzam; and my number one fan and wonderful sister, Shams Al-Azzam.

I also want to dedicate this to my grandparents (Ismael and Layla), who one passed away during my PhD. Both provided me with warmth and love and witnessed me grow into an accomplished and ambitious woman.

I want to also dedicate this to my friends Arlina de Lugo and Bailee Hunter for being such amazing friends throughout the years and for being such caring and loving sisters.

Lastly, I want to dedicate this to my pet cat, another cherished family member, Massimo, a loving and affectionate companion.

TABLE OF CONTENTS

LIST OF FIGURES

LIST OF TABLES

ACKNOWLEDGEMENTS

I would like to acknowledge Professor Gene Yeo for their support as the chair of my committee. Through multiple drafts and many long nights, their guidance has proved to be invaluable.

I want to thank also the individuals that have helped in the project and had a very large impact on my PhD, Jenny To, Vaishali Gautam, Lena Street, Chloe Nguyen, Jack Naritomi, and Dylan Lam. I want to also thank PIs I collaborated with Uri Manor, Jeffrey D. Rothstein, Alyssa Coyne, and Marko Jovanovic.

Chapter 1 and Chapter 2, in full, is has been accepted in Neuron and will be published in the next couple of months.

Chapters 1 and 2 are a full reprint of material as it will appear in: Jenny To, Vaishali Gautam, Lena Street, Chloe Nguyen, Jack Naritomi, Dylan Lam, Uri Manor, Jeffrey D. Rothstein, Alyssa Coyne, and Marko Jovanovic. Inhibition of RNA splicing triggers CHMP7 nuclear entry, impacting TDP-43 function and leading to the onset of ALS cellular phenotypes. *In revision.* The dissertation author was the primary investigator and author of this paper.

VITA

2018 Bachelor of Science in Biology, University of California San Diego

2019 Master of Science in Biology, University of California San Diego

2024 Doctor of Philosophy in Neuroscience, University of California San Diego

PUBLICATIONS

Al-Azzam, N.*, Sison, S.*, Khachatryan, A., Estrada, E., Nguyen, C., To, J., Somalinga, B., & Yeo, G. W. (in preparation). Small-molecule modulation of CAG RNA interactors as potential drug targets for Huntington's disease. *(Co-first authors)* Manuscript in preparation.

Pessentheiner, A. R., Y., C.-J., Tognaccini, C., Labib, C., **Al-Azzam, N.**, Jessen, F., Trieger, G., Secrest, P., Majithia, A., & Gordts, P. L. S. M. (2024). Impaired mitophagy in Sanfilippo A mice causes hypertriglyceridemia and brown adipose tissue activation. Under review at *Nature Communications*

Al-Azzam, N., To, J., Gautam, V., Street, L., Naritomi, J., Nguyen, C., Lee, B., Jovanovic, M., & Yeo, G. W. (2024). Inhibition of RNA splicing triggers CHMP7 nuclear entry, impacting TDP-43 function and leading to the onset of ALS. Under review at *Multi-Cell*.

Street, L., Rothamel, K., Brannan, K., Jin, W., Bokor, B., Dong, K., Rhine, K., Madrigel, A., **Al-Azzam, N**., Kim, J., Ma, Y., Abdou, A., Wolin, E., Doron-Mandel, E. W., Ahdout, J., Mujumba, M., Jovanovic, M., & Yeo, G. W. (2023). Large-scale map of RNA binding protein interactomes across the mRNA life-cycle. *bioRxiv*. DOI: 10.1101/2023.06.08.544225.

Rhine, K., **Al-Azzam, N**., Yu, T., & Yeo, G. W. (2022). Aging RNA granule dynamics in neurodegeneration. *Frontiers in Molecular Biosciences*, 9, Article 991641. DOI: 10.3389/fmolb.2022.991641.

Tillo, M., Lamanna, W. C., Dwyer, C. A., Sandoval, D. R., Pessentheiner, A. R., Al-Azzam, N., Sarrazin, S., Gonzales, J. C., Kan, S. H., Andreyev, A. Y., Schultheis, N., Thacker, B. E., Glass,

C. A., Dickson, P. I., Wang, R. Y., Selleck, S. B., Esko, J. D., & Gordts, P. L. S. M. (2022). Impaired mitophagy in Sanfilippo mice causes hypertriglyceridemia and brown adipose tissue activation. *Journal of Biological Chemistry*, 297(4), Article 101029. DOI: 10.1074/j.jbc.2022.102159.

ABSTRACT OF THE DISSERTATION

Unraveling RNA-Binding Protein Mislocalization in Neurodegenerative Disorders

by

Norah Al-Azzam

Doctor of Philosophy in Neuroscience

University of California San Diego, 2024

Professor Gene Yeo, Chair

Mislocalization of RNA-binding proteins (RBPs) is a hallmark of neurodegenerative diseases like ALS, where the abnormal distribution of RBPs disrupts cellular functions. TDP-43, typically found in the nucleus, accumulates in cytoplasmic inclusions in ALS neurons, impairing RNA metabolism and leading to neurodegeneration. ALS is also linked to reduced nucleoporins and increased nuclear CHMP7, a protein that damages nuclear pores. Using CRaft-ID, we identified 55 RBPs that affect CHMP7 localization, focusing on SmD1, a component of the SMN complex. We found that CHMP7 interacts with SmD1 and related proteins in an RNA-sensitive

manner and observed reduced SmD1 in ALS iPSC-derived motor neurons (MNs). Inhibiting SmD1/SMN increased nuclear CHMP7, while overexpressing SmD1 restored CHMP7 localization and STMN2 splicing. These findings highlight early ALS pathogenesis driven by SMN complex dysregulation.

INTRODUCTION

The compartmentalization of cellular contents into membrane-bound organelles is a long-established paradigm in biology. However, recent evidence demonstrates that lipid membranes are not strictly required to segregate macromolecules into distinct structures. Instead, discrete liquid phases—like oil in water—may form when proteins containing intrinsically disordered regions (IDRs) bind to RNA, forming multimeric complexes. These multimeric complexes eventually support a phase transition, in which a dense proteinaceous granule forms by liquid-liquid phase separation (LLPS). A variety of cytoplasmic liquid-like granules form via LLPS, including stress granules (SGs), P bodies, G bodies, and others (Banani et al., 2017).Importantly, many of these granules are seeded in response to stress, and they are disassembled once the stress event ends (Buchan et al., 2008; Wheeler et al., 2016; Jin et al., 2017). However, a granule may persist beyond the stress event if it undergoes a material transition into a solid- or gel-like status (Zhang et al., 2019; Lu et al., 2021). When granules mature into gels, they have reduced interactions with the surrounding cellular milieu and can further transition into fibrils or other aggregated structures (Patel et al., 2015). Solid- or gel-like granules are disastrous for neurons, most of which are not replenished throughout an organism's lifetime (Lim and Yue, 2015). Dysregulation of the material state of cellular granules is linked with a variety of neurodegenerative diseases, including amyotrophic lateral sclerosis (ALS), Huntington's, Alzheimer's, and others (Patel et al., 2015; Li et al., 2016; Wegmann et al., 2018).

RNA is a critical component of phase-separated granules. Many proteins that are enriched within granules contain not only IDRs but also canonical RNA-binding domains (Markmiller et al., 2018). These RNA-binding proteins (RBPs) can therefore multimerize with themselves via IDRs and RNA via their RNA-binding domains (Rhine et al., 2020b). Biochemical studies demonstrate that RNA can reduce the amount of protein needed to form

proteinaceous droplets *in vitro* (Kato et al., 2012; Molliex et al., 2015; Niaki et al., 2020; Yang et al., 2020), and elegant cellular experiments are consistent with the idea that cytoplasmic RNA promotes LLPS (Fuller et al., 2020; Bauer et al., 2022). Conversely, an overabundance of RNA may buffer phase separation by diluting multimeric interactions among many RNA and RBP molecules, though this phenomenon is more pronounced in the nucleus (Maharana et al., 2018). The cytoplasmic concentration of RNA can be tuned by stress events, especially translational arrest at polysomes that cause an acute increase in available RNA for RBP binding (Bounedjah et al., 2014; Iserman et al., 2020). In general, longer RNAs are more effectively recruited into granules, but biases toward certain sequence or structure motifs heavily depend on the RBP recognizing the RNA molecule and other polymers in the cell (Khong et al., 2017; Hallegger et al., 2021; Rhine et al., 2022a). Repetitive RNAs may also contribute to granule formation independently of proteins by undergoing self-associations like those found in G-quadruplexes (Boeynaems et al., 2019).

Aside from promoting granule formation, RNA also alters the viscoelastic properties of granules (Roden and Gladfelter, 2021; Laghmach et al., 2022). As mentioned above, RNA promotes RBP multimerization by acting as a scaffold to which proteins may bind (Schwartz et al., 2013; Rhine et al., 2020a). Scaffolds naturally stabilize the resulting condensate (Decker et al., 2022; Sanchez-Burgos et al., 2022), which can accelerate coarsening into solid- or gel-like material states (Bose et al., 2022). In addition, the physical interaction between RNA and its cognate proteins may lead to conformational rearrangements in the protein that shield certain domains, inhibiting efficient dissolution by chaperones that resolve granules (Yoshizawa et al., 2018). Finally, mutations in RBPs can further promote solid-like transitions (Zhu et al., 2014; Niaki et al., 2020). Indeed, many mutations identified in ALS affect RBPs containing

IDRs, including FUS, TDP-43, hnRNPA1, and others (Sreedharan et al., 2008; Vance et al., 2009; Kim et al., 2013). RNA promotes condensation of all these proteins, indirectly supporting an aberrant material state transition consistent with inclusions found in neurodegeneration patients.

Therefore, RNA has a critical role in establishing the biophysical properties of condensates. Given the vast number of biological processes that require RNA, sequestration of RNA into disease-associated granules is an inherently perturbative outcome that destabilizes cellular homeostasis and eventually promotes cell death (Pushpalatha et al., 2022). In the following sections, I review the various regulatory and biophysical processes that contribute to RNA granule aging, especially in the context of neurodegeneration as persistent RNA granules disrupt cellular homeostasis. I also present various techniques that may be used to further our understanding of how RNA impacts granule maturation.

Turnover of stress granules in health and disease

The normal life cycle of a stress granule involves rapid formation and quick dissolution regulated by several mechanisms. Upon different stress conditions, multiple pathways including inhibition of mTOR, phosphorylation of eIF2a and disruption of eIF4F complex induce SG formation (Harding et al., 2000; Gilks et al., 2004; Thedieck et al., 2013). All three pathways converge to stall and disassemble polysomes, which is arguably the common trigger of SG formation (Buchan and Parker, 2009). When SGs form, RBPs and mRNA molecules play a major role. Two RBPs, in particular, have been thoroughly studied for the assembly of cytoplasmic SG: T-cell intracellular antigen 1 (TIA-1) and Ras-GTPase-activating protein SH3-domain-binding protein 1 (G3BP1) (Tourriere et al., 2003; Gilks et al., 2004). G3BP1 and its homolog G3BP2 are the core components of stress granules (Figure 1), which undergo RNA-

dependent LLPS by sequestering free RNA to generate protein-RNA condensates (Guillen-Boixet et al., 2020; Yang et al., 2020). G3BP1 can also interact with many IDR-containing RBPs, including Caprin-1 and TIA-1, and both promote G3BP1/2-mediated LLPS (Guillen-Boixet et al., 2020; Yang et al., 2020). The size and liquid properties of RNA-protein condensates in cells are affected by RNA recruitment (Garcia-Jove Navarro et al., 2019; Roden and Gladfelter, 2021). Furthermore, the availability of RNA–RNA assemblies is important for granule assembly *in vitro* (Van Treeck et al., 2018). Trcek *et al.* demonstrated in *Drosophila* germ cells that different mRNA features govern mRNA localization to granules and self-assembly within granules; they noted that localization is encoded by specific RNA regions, whereas self-assembly is RNA sequence-independent (Trcek et al., 2020).

Canonical RNA turnover in SGs occurs in a stepwise manner (Wheeler et al., 2016). First, translation is slowed during stress, and polysomes release their respective messenger ribonucleoproteins (mRNPs). The free mRNP particles oligomerize via protein-protein, protein–RNA, or RNA–RNA interactions. When more RNAs enter the non-translating pool, oligomers form stable core assemblies (Decker et al., 2022). As a result of fusion and mRNP recruitment, a mature SG with a distinct core-shell substructure is generated. Even mature SGs (especially the "shell") are still in dynamic equilibrium, exchanging materials with polysomes and P bodies (Wheeler et al., 2016). It is worth noting that a recent super-resolution imaging study showcased comparable translation efficiency of their reporter in SGs over outside of SGs, suggesting that the SG environment is not inhibitory to translation and that global translation inhibition in response to stress is more likely to be upstream of rather than the consequence of SG formation (Mateju et al., 2020). SGs begin to break down via shell loss followed by core dispersal, and mRNPs re-enter translation. Translationally-stalled mRNAs are titrated out of SGs, producing

structural instability in the protein complexes and eventually gradual deconstruction of the visible SGs (Wheeler et al., 2016). Several lines of evidence have shown that RNA can mitigate excessive protein-protein interactions, which lead to pathological aggregates seen in a variety of neurodegenerative disorders (Maharana et al., 2018; Mann et al., 2019; Zacco et al., 2019), emphasizing the critical balance between protein-protein, RNA–protein, and RNA–RNA interactions required for proper SG assembly and disassembly. Post-translational modifications also play a critical role in SG disassembly, Maxwell *et al.* revealed an important function of heat-induced polyubiquitylation, which is instrumental in preparing cells for the restart of cellular activities upon stress release (Maxwell et al., 2021). Furthermore, the SG scaffold protein G3BP1 is a key substrate for polyubiquitin-dependent disassembly of heat-induced SGs (Gwon et al., 2021). One crucial mechanism in this recovery phase is the restart of translation, which is accompanied by the ubiquitin-dependent disassembly of SGs (Maxwell et al., 2021). Lastly, increased recruitment of small ubiquitin-like modifier ligases into the SGs is observed upon stress exposure leading to SUMOylation of proteins necessary for SG disassembly (Marmor-Kollet et al., 2020).

RNA helicases also have a major role in RNA granule dynamics and could contribute to the interconnection between mRNA storage, translation, and decay (Hondele et al., 2019; Weis and Hondele, 2022). Recent work shows that assembly and disassembly of RNA granules are monitored by DEAD-Box helicase 6 (DDX6), an essential P body component, in neuronal maturation both *in vitro* and *in vivo* (Bauer et al., 2022). ATP, which is consumed by RNA helicases, is required for the fast construction, remodeling, and disassembly of stress granule components (Wolozin and Ivanov, 2019). Furthermore, DDX6 granule condensation requires Staufen-2-dependent RNA interaction during synaptic inhibition. This is most likely owing to

Stau2's participation in mRNA transport and redistribution (Bauer et al., 2022). In addition, recent work has shown that sex chromosome-encoded RNA helicases such as DDX3X and DDX3Y influence the formation of RNA granules in an ATP-independent manner but have different LLPS propensities (Shen H. et al., 2022).

Nuclear import of granule-associated proteins is another important layer of SG regulation (Guo et al., 2018), and defects in nucleocytoplasmic transport are a significant pathogenic factor in ALS (Zhang et al., 2015; Gleixner et al., 2022). Cytoplasmic protein clumps, which are frequently observed in many neurodegenerative illnesses, impair nucleocytoplasmic transport, implying that abnormalities in nucleocytoplasmic transport might constitute a general cause of neurodegeneration (Hutten and Dormann, 2020; Gonzalez et al., 2021; Odeh et al., 2022). Critical nucleocytoplasmic transport components such as karyopherins (importins and exportins), Ran GTPase, and nucleoporins translocate to stress granules in response to cellular stress, resulting in inefficient nucleocytoplasmic transport (Zhang et al., 2018). Importantly, in C9ORF72 ALS models, blocking stress granule construction decreases these abnormalities as well as neurodegeneration (Zhang et al., 2018). These discoveries linked two pathophysiological processes, stress granule construction and nucleocytoplasmic transport disruption, into a single pathway that leads to pathogenesis. Thus, an intriguing issue of the present work is analyzing how changes to essential stress granule components or remodeling machinery affect the various phases of this assembly and disassembly process.

RNA promotes the maturation of granules to solid-like material states

Following granule formation, the cell has a variety of mechanisms to promote dissolution of granules, including posttranslational modifications that signal for turnover of critical RBPs, expression of chaperones that recognize granule proteins, and helicase activity that ejects RBPs

from RNA (Guo et al., 2018; Hondele et al., 2019; Maxwell et al., 2021). However, complete resolution of RNA granules may not be possible if the granule has coarsened into a solid- or gel-like state (Figure 1). Many *in vitro* studies demonstrate the effect of aging, but there are two separate biophysical processes through which a granule may achieve a solid- or gel-like state. A recent study by Jawerth *et al.* proposed that condensates do not become gels *per se* and instead behave as a Maxwell fluid with strongly increasing viscosity as a function of condensate age (Jawerth et al., 2020). Other studies indicate that RBPs bound to RNA may undergo dynamical arrest via percolation, halting exchange with the surrounding dilute phase (Harmon et al., 2017; Rhine et al., 2020a; Choi et al., 2020; Bose et al., 2022; Linsenmeier et al., 2022; Mittag and Pappu, 2022). Granules may also partially transition to gels, as was observed with the RBP FUS (Shen Y. et al., 2022). In principle, these mechanisms likely arrive at the same outcome: an RNA granule that is resistant to dissolution because of a change in its material properties.

Many neurodegenerative diseases are linked to the formation of fibrils or solid-like inclusions (Kim et al., 2013; Nomura et al., 2014; Bowden and Dormann, 2016; French et al., 2019), which have similar material properties to aged RNA-containing SGs (Zhu et al., 2014; Patel et al., 2015; Murray et al., 2017; Fonda et al., 2021). Proteins associated with ALS (FUS, TDP-43, hnRNPA1, etc.), Alzheimer's (Tau), and Parkinson's (α-synuclein) undergo both LLPS and aggregation into fibers (Gotz et al., 2001; Roberson et al., 2007; Sreedharan et al., 2008; Vance et al., 2009; Kim et al., 2013; Wegmann et al., 2018; Ray et al., 2020). Although fibers are thought to be the causative agent of disease, certain ALS-associated RBPs incorporate into liquid-like stress granules (Bentmann et al., 2012; Markmiller et al., 2018; Reber et al., 2021; An et al., 2022). ALS-linked mutations in these RBPs accelerate the granule aging process or inhibit recognition by protein chaperones (Guo et al., 2018; Hofweber et al., 2018; Niaki et al., 2020).

Aged RNA granules can be deleterious on their own by stalling translation via RNA sequestration and by preventing cellular recovery from stress (Reineke and Neilson, 2019; Pushpalatha et al., 2022). Disease-linked mutations cause some proteins like TDP-43 to bypass the liquid phase altogether, forming aggregates or fibrils at physiological concentrations (Patel et al., 2015; Cao et al., 2019; Mathieu et al., 2020). In these cases, LLPS may act as a protective agent to prevent or decelerate deleterious solid- or gel-like transitions.

Recent evidence highlights the role of RNA in promoting the transition of granules to solid-like material states. The most common genetic cause of ALS—a repeat expansion of the C9ORF72 locus—leads to the expression of the highly toxic $(GGGGCC)_n$ RNA motif and translation of repetitive dipeptide chains, especially poly-RG and poly-PR (DeJesus-Hernandez et al., 2011). Importantly, this RNA repeat engages in multivalent base pairing, promoting granules that transition into a gel-like state (Jain and Vale, 2017). Other disease-associated RNA repeats also impact granule aging *in vitro* (Ma et al., 2022), and the self-association of G-rich RNA forms solid-like fibers (Boeynaems et al., 2019). Normal mRNA sequences may also contribute to RNA self-assembly or gelation, as has been observed in worms and flies (Lee et al., 2020; Trcek et al., 2020). It is possible that P-body-associated RNA helicases are required for proper resolution of multivalent RNA tangles (Hondele et al., 2019; Majerciak et al., 2021; Linsenmeier et al., 2022), which can age condensates into gels. Together, these studies demonstrate that RNA can promote solid- or gel-like transitions in RNA granules, and sequencing-based technologies like CLIP-seq and others may help identify changes in RNA biology during disease (Van Nostrand et al., 2016; Hallegger et al., 2021; Wollny et al., 2022) (Table 1.1). Although we do not yet know how exactly aged RNA granules and fibers lead to cell death, the next section will discuss how the persistence of aged granules and fibers may disrupt cellular homeostasis.

Persistent granules disrupt cellular homeostasis and could potentially serve as therapeutic targets

The persistence of RNA granules may disrupt cellular homeostasis through multiple mechanisms, including posing as a cytotoxic stimulus, sequestering proteins important for maintaining cellular homeostasis, and altering SG assembly and disassembly (Figure 1). In Alzheimer's disease, amyloid-beta aggregates stimulate persistent SGs (Ghosh and Geahlen, 2015), and SG assembly promotes the phosphorylation of tau (Vanderweyde et al., 2012), potentially accelerating the onset of neurodegeneration. In the case of multiple polyglutamine (polyQ) diseases like Huntington's, the polyQ aggregates could trigger various types of stresses (Labbadia and Morimoto, 2013; Matos et al., 2019), including misfolded protein stress. The polyQ aggregates also sequester SG components (Uchihara et al., 2001; Furukawa et al., 2009; Sleigh et al., 2020), leading to aberrant SG composition. These SGs contain misfolded proteins, further sequestering components of autophagy (Mateju et al., 2017). As one of the SG clearance pathways (Ryu et al., 2014), impaired autophagy could in turn disrupt the disassembly of SGs. In ALS, SGs colocalize with TDP-43 and poly-GR aggregates (Liu-Yesucevitz et al., 2010; Chew et al., 2019), and chronic SGs could directly contribute to ALS onset (Daigle et al., 2016; Zhang et al., 2019). The poly-PR aggregates could directly interact with ribosomes and impair protein translation (Zhang et al., 2018). Global splicing and RNA localization may also be altered due to the sequestration of important regulators in these cellular processes (Charizanis et al., 2012; Markmiller et al., 2021).

The unique formation of persistent granules in these neurodegenerative diseases enables the development of new strategies for therapeutic treatment. antisense oligonucleotides and RNA-targeting CRISPR have been demonstrated to eliminate toxic RNA granules (Lee et al.,

2012; Batra et al., 2017) when particular RNAs are known to form these granules. Small molecule drugs could potentially be developed to target specific proteins responsible for the assembly or preventing disassembly of persistent granules. More efforts are needed to better depict the components of these granules under different disease conditions (Table 1). Meanwhile, explorative drug screens could be performed to repurpose existing drugs for resolving persistent granules in different disease contexts (Fang et al., 2019).

Technologies for investigating RNA granules

Pioneering research has laid the groundwork for our present understanding of RNA granules in neurodegenerative disease, expanding our understanding of the fundamental mechanisms of granule assembly and disassembly, as well as their composition and structural organization. However, there remains many gaps in the field. To conclude, we review new methods to aid our understanding of RNA granules (Table 1.1).

Over the past decades, there have been a variety of different approaches and methods to characterize and identify different stress granule components and functions (Table 1.1). A starting point of analysis for any granule-associated client protein is to identify its components with imaging technology. Initially many components of stress granules were identified using specific antibodies via immunofluorescence or immunohistochemistry. These imaging-based experiments detected several different types of stress granule components, including RBPs and translation machinery components. Recent advances in microscopy enable robust live-cell imaging of diffusing granule proteins, providing biophysical data of granule material properties. Fluorescence *in situ* hybridization and the MS2 tagging system can be used for fixed and live tracking of RNAs (Le et al., 2022).

Alternatively, omics-based techniques identify components of the proteome and transcriptome of RNA granules. Previously published work from our lab used ascorbate peroxidase (APEX2) proximity labeling to identify components of SGs in human cells (Markmiller et al., 2018). APEX can also be repurposed to pull down RNAs instead of proteins (Padron et al., 2019). Other techniques such as BioID provide similarly robust datasets of the granule proteome (Youn et al., 2018). We have also pioneered enhanced CLIP technologies, which identify bound RNAs in granules (Van Nostrand et al., 2016; Corley et al., 2020; Blue et al., 2022). Coupling these technologies with different biological conditions can identify stress-responsive changes in granule components, including shifts that are precursors to neurodegeneration (Markmiller et al., 2021).

Biochemical techniques allow the most robust characterization of granules properties and even enable the purification of whole granules from cells. Matheny *et al.* compared two granule isolation methods, and they demonstrated that more SG enrichment comes from differential centrifugation and immunopurification (Matheny et al., 2019). The RNAs from purified granules were similar to the RNAs found in the cellular granules confirmed with FISH. Biophysical techniques such as FRAP and microrheology also identify the material properties of *in vitro* and *in vivo* granules, which may help pinpoint the transition from a normal granule to a disease-associated granule. Overall, the approaches discussed here give a wealth of information for understanding stress granule production and disassembly, function, and regulation, which we anticipate will be important for identifying how and why RNA granules transition into neurodegeneration-linked fibers.

Conclusion

Sequestering critical RBPs and RNA molecules into granules is an inherently risky maneuver for cells. If a cell does not pause translation, splicing, and other energetically expensive processes, it may not survive the stress event. However, if the stress response persists for too long, the cell may permanently entangle essential machinery for translation, splicing, and other processes into granules. As I discussed above, persistent granules may undergo a phase transition into nondynamic, solid- or gel-like structure, which is a hallmark of neurodegenerative diseases. Therefore, it is necessary to better understand how and why RNA granules mature into nonresolvable aggregates so that we can develop appropriate remedies to counteract deleterious phase transitions.

TABLE 1.1. Imaging, sequencing, and biochemical methods for studying RNA granules.

	Method	Approach	Advantage	Disadvantage	References
Imaging techniques	Immunofluorescence/ tagging with fluorescent protein	Colocalization with granule markers	Technically straightforward; quantitative measurement of partition coefficients	Low throughput, requires prior knowledge of granule proteins, use of fixatives may alter granule properties	Irgen-Gioro et al. (2022)
	Single particle/molecule tracking (SPT/SMT)	Substoichiometric labeling of proteins with photostable fluorophores for single-particle tracking *in vivo*	Compatible with IF/tagging methods above; live imaging under various conditions	Requires super resolution imaging, labeling; may disrupt the localization of the original transcripts or proteins	(Li et al., 2016; Horvathova et al., 2017; Mateju et al., 2020; Moon et al., 2020)
	RNA-fluorescence *in situ* hybridization (FISH)/ Single-molecule FISH (smFISH)	Hybridization-based method to label RNAs with fluorescent probes	Compatible with IF, quantitative, feasible to multiplex	Costly, require prior knowledge, use of fixative may alter granule properties	(Ivanov et al., 2011; Zurla et al., 2011; Khong et al., 2017)
Omics techniques	APEX proximity labeling (APEX2)	APEX2 protein fusion labels nearby proteins and RNAs when biotin-phenol and hydrogen peroxide are added	Creates a snapshot of proteins and RNAs in proximity to a protein of interest (suitable for studying dynamics)	Partitioning and diffusion of proteins within stress granules increases noise and background	(Markmiller et al., 2018; Padron et al., 2019; Elmsaouri et al., 2022)
	Bio-ID/TurboID	BirA mutant fused to protein of interest biotinylate the proteins in close proximity in living cells	Accumulated labeling in a period of time (also suitable for transitory interactors)	Partitioning and dynamics of proteins within stress granules increases noise and background, cannot label RNA	(Roux et al., 2012; Kim et al., 2016; Youn et al., 2018)
	CLIP-Seq	Immunoprecipitation of crosslinked RBP-RNA interactions; sequencing of RNA molecules with Illumina methodology or equivalent	Allow base-resolution identification of RBP binding sites on target RNAs, compatible with proximity labeling (Proximity-CLIP)	Requires IP-grade antibodies	(Niranjanakumari et al., 2002; Van Nostrand et al., 2016; Benhalevy et al., 2018)
Biochemical/ biophysical techniques	RNP granule purification	Fractionation of RNP granules by ultracentrifugation, followed by immunoprecipitation of granule markers	Compatible with various downstream analyses, including mass spec and RNA-Seq	Loses weakly associated proteins and RNAs in the "shell" of the granule	Matheny et al. (2019)
	Fluorescence recovery after photobleaching (FRAP)	Intense photobleaching of granules; tracking of fluorescence recovery over time	Can help determine viscoelastic properties of granules	Recovery may be due to internal or external diffusion, so the parameters need to be decoupled; bleaching laser apparatus needed	(Ganser and Myong, 2020; Rhine et al., 2022b)
	Microrheology	Beads within granules are used to determine the diffusion within the condensate	Determines the internal diffusion coefficient, which is used to calculate the viscoelastic properties of the granule	Rheology is technically difficult to establish in a cell	Elbaum-Garfinkle et al. (2015)

Chapter 1 Charged multivesicular body protein 7 (CHMP7) novel role in RBP biology

Amyotrophic lateral sclerosis (ALS) is a severe neurodegenerative disease characterized by the progressive degeneration of both upper and lower motor neurons, resulting in the loss of motor function, respiratory failure, and ultimately death (Wijesekera and Nigel Leigh, 2009; Taylor et al., 2016). While the etiology of ALS remains multifaceted and poorly understood, recent research has shed light on a new aspect of its pathogenesis.

Nucleoporins, essential components of the nuclear pore complex (NPC), have been observed to be diminished in up to 90% of sporadic ALS (sALS) cases (Zhang et al., 2015; Coyne et al., 2021; Hayes et al., 2020; D'Angelo et al., 2009). Recent studies have identified that the abnormal nuclear localization of charged multivesicular body protein 7 (CHMP7), a component of the ESCRT-III degradation pathway, causes NPC injury (Coyne et al., 2021). This intriguing discovery highlights the critical roles of CHMP7 and the NPC in ALS pathogenesis, prompting further investigation into the regulatory mechanisms governing CHMP7 localization and its potential as a therapeutic target. In this study, we elucidate the intricate molecular pathways linking nucleoporin deficiency to aberrant CHMP7 nuclear localization by identifying Survival of Motor Neuron (SMN) complex dysfunction as an unexpected contributor to the onset and progression of sporadic ALS.

In the cytoplasmic phase of small nuclear ribonucleoprotein particle (snRNP) biogenesis, the SMN protein complex plays a critical role as an assembly factor (Yi et al., 2020). Its primary function is to facilitate the efficient and specific binding of the heteroheptameric Sm complex to a conserved binding site found on the spliceosomal U1, U2, U4, and U5 snRNAs. This intricate process relies on the coordinated actions of various proteins within the SMN-Gemin protein complex (Tang et al., 2016; Xu et al., 2016). The SMN-Gemin complex is a multiprotein

assembly that comprises a minimum of eight core polypeptides and an additional seven substrate polypeptides known as Sm/LSm proteins (Pillai et al., 2003; Meister et al., 2001). Together, these proteins collaborate to orchestrate the precise assembly of snRNPs in the cytoplasm (Will and Lührmann, 2001). This assembly process involves the stepwise addition of Sm proteins to snRNA, culminating in the formation of functional snRNPs that are integral to the splicing of pre-messenger RNA (pre-mRNA) in the nucleus of eukaryotic cells. SmD1, along with six other snRNP proteins (SmB, SmD2, SmD3, SmE, SmF, and SmG), forms a heptameric ring structure crucial for the assembly of snRNPs, which surround U-rich snRNAs and play a pivotal role in pre-mRNA splicing (Patel and Steitz, 2003). Depletion of SmD1 can disrupt the SM-SM interaction, disrupting the formation of complex with SMN, and subsequently decreasing the levels of U1, U2, U4, and U5 snRNPs (Mandelboim et al., 2003; Grimm et al. ,2013). These findings underscore the essential role of Sm proteins in splicing, snRNA maturation, and stability (Massenet et al., 2002).

Dysregulation or mutations in the SMN complex have been associated with various neurodegenerative diseases, such as spinal muscular atrophy (SMA), underscoring its significance in both development and disease (Liu et al., 1997; Harada et al., 2002). Recent investigations have further highlighted its relevance in the pathogenesis of ALS, especially in sporadic cases (sALS) (Shukla and Parker, 2016). TDP-43 knockout mice (Shan et al., 2010), and mutant SOD1 mice also exhibit Gemin deficiency (Gertz et al., 2012). Furthermore, Gemin deficiency exacerbates cellular stress and degeneration in ALS (Shan et al., 2010; Tsuiji et al., 2013). Building on this context, through an unbiased image-based CRISPR screen using the CRaft-ID (CRISPR-based microRaft followed by guide RNA identification) workflow (Wheeler et al., 2020), we have identified RNA processing proteins, particularly those integrated into the

SMN-core complex, as critical regulators of CHMP7 subcellular localization. Confirming our findings, depletion of core SMN complex components results in nuclear localization of CHMP7. As previously established, Sm complex proteins and CHMP7 utilize the exportin protein XPO1 for active transport from the nucleus to the cytoplasm (Fornerod and Ohno, 2002; Vietri et al., 2020). We demonstrate that CHMP7 interacts with SMN complex proteins in motor neurons. This interaction is mirrored at the RNA level, with CHMP7 binding to snRNAs and mRNAs encoding constitutive and alternative splicing factors. We observe reduced expression of SmD1, a core component of the SMN complex in sporadic ALS (sALS) iPSC-derived motor neurons (MNs). As CHMP7 nuclear localization causes NPC injury (Coyne et al., 2021), leading to the loss of nuclear TDP-43 and reduced levels of STMN2 protein (Krus et al., 2022; Melamed et al., 2019; Klim et al., 2019), we show that restoration of SmD1 levels in sALS iPSC-MNs returns CHMP7 to the cytoplasm, and corrects regulation of STMN2 protein. Collectively, our findings suggest the existence of an early pathway involving dysregulation of the SMN core complex, which drives the initial stages of sporadic ALS pathogenesis.

Image-based genome-wide CRISPR screen technology identifies modulators of CHMP7 nuclear localization.

To identify genes that modulate the subcellular localization of CHMP7, we employed the CRaft-ID imaging-based screening and analysis workflow to evaluate a lentiviral library with >12,000 sgRNAs targeting over 1,000 annotated RNA binding proteins (RBPs) (Wheeler et al., 2020). Two HeLa cell-lines expressing an endogenously GFP tagged CHMP7 and stably integrated GFP-CHMP7 were transduced with the lentivirus-packaged library at low multiplicity of infection and sparsely seeded on Cell Microsystems CytoSort arrays, each containing 40,000 “microRafts” (100x100 μm). A total of 12 microRaft arrays seeded at 20% cell occupancy were

imaged and 84 individual microRafts containing cells with nuclear localized CHMP7-GFP were isolated using the CellRaft AIR System. Cells from candidate rafts were assigned a unique barcode by targeted PCR of the sgRNA insert and pooled for NGS sequencing after gel extraction and cleanup (Supplementary Figure 1A, 1B). For reference, we picked a representative library containing the six pooled rafts and ran on the Agilent Tapestation for gel extraction between 220-250 bp (Supplementary Figure 1C). The final DNA library was subjected to sequencing on the Miseq (Illumina) platform and the identities of the sgRNAs were extracted by the CRaft-ID software package (Figure 1A). The Model-based Analysis of Genome-wide CRISPR-Cas9 Knockout (MAGeCK) algorithm (Li et al., 2014) was used to identify statistically significantly enriched sgRNAs. We successfully identified 73 guides (from 84 rafts), 55 candidate genes (Figure 1B) of which some are involved in RNA processing steps such as in RNA splicing (SNRPD1/SmD1, NOVA2) and mRNA translation (EIF2AK2, EIF4G2, EIF2AK4) (Figure 1C, Supplementary Figure 1D).

Figure 1.1: Image-based genome-wide CRISPR screen technologies identifies modulators of CHMP7 nuclear localization.

A. Schematic of the pooled experiment used in the proof-of-concept study. Cell culture workflow for CRaft-ID. A CRISPR–Cas9 gRNA library was generated from an array of sgRNA oligonucleotides cloned into the lentiCRISPR v2 backbone. HeLa cells were infected at low multiplicity of infection (MOI .15) and cultured in bulk for 7 d after selection, allowing lethal guides to drop out of the pool. A bulk infection of cells with a gRNA library targeting over 1,000 annotated proteins (>12,000 sgRNAs) was performed, followed by single cell plating on 12 microRaft arrays to screen genetic knockout clones for mislocalization of CHMP7. Our gRNA library is the same design as those traditionally used for pooled CRISPR screens and requires no library modifications, making this workflow amenable to existing CRISPR gRNA libraries (Wheeler et al., 2020). Cells were plated on microRaft arrays and grown at low density and a live DAPI stain was added to each raft. Positive candidates, where GFP is in the nucleus and co-localizing with DAPI, were selected. To sequence the sgRNA associated with CHMP7 mislocalization to the nucleus, we isolated target colonies adhered to microRafts from the array. A motorized microneedle, fitted over the microscope objective, was actuated to pierce the PDMS microarray substrate and dislodge individual magnetic microRafts from the array. Released microRafts and their cargo were collected with a magnetic wand into a strip tube containing a lysis buffer for a targeted two-step PCR with in-line barcodes, followed by high-throughput sequencing.
B. Bar chart showing the total number of rafts picked (84), sequenced (73 with successfully obtained PCR products), identified (55 using CRaft-ID), and proteins confirmed by siRNA depletion (23). The pie chart represents the distribution of sgRNAs identified from each isolated cell.
C. GO molecular function analysis of n = 55 proteins identified that were depleted in the screen as compared to input of total CRISPR screen candidates and total HeLa cell RNA-seq (https://metascape.org)

Figure 1

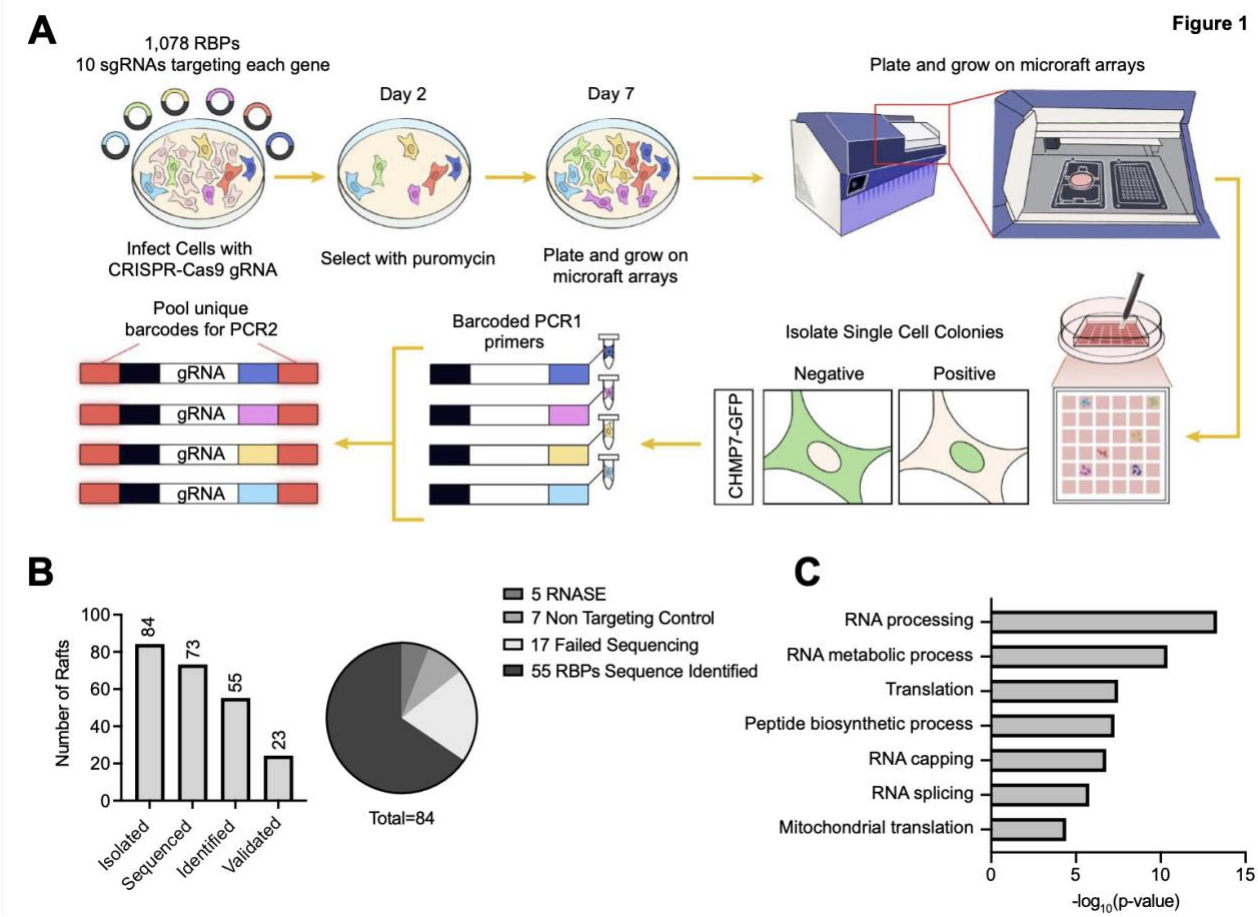
A
1,078 RBPs
10 sgRNAs targeting each gene
Infect Cells with CRISPR-Cas9 gRNA
Day 2
Select with puromycin
Day 7
Plate and grow on microraft arrays
Plate and grow on microraft arrays
Isolate Single Cell Colonies
Negative
Positive
CHMP7-GFP
Barcoded PCR1 primers
Pool unique barcodes for PCR2
gRNA
gRNA
gRNA
gRNA
B
Number of Rafts
100
80
60
40
20
0
84
73
55
23
Isolated
Sequenced
Identified
Validated
5 RNASE
7 Non Targeting Control
17 Failed Sequencing
55 RBPs Sequence Identified
Total=84
C
RNA processing
RNA metabolic process
Translation
Peptide biosynthetic process
RNA capping
RNA splicing
Mitochondrial translation
0
5
10
15
-log10(p-value)

Supplementary Figure 1

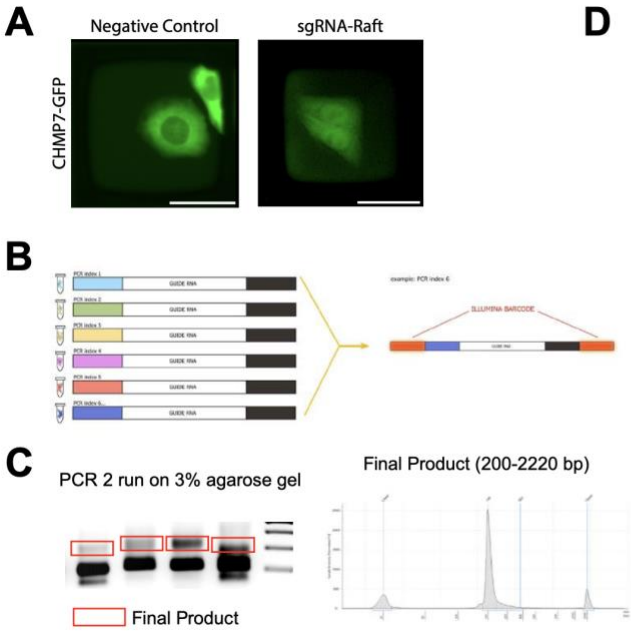

D

Name	Function
AAVS1	Genetic Locus
ABT1	small-subunit processome assembly
ADAT2	ADAT2 tRNA wobble adenosine to inosine editing
CPEB2	Negative regulation of cytoplasmic translational elongation
CLK1	Peptidyl-threonine phosphorylation
CWC27	protein peptidyl-prolyl isomerization
DDX10	rRNA processing
DDX26B	snRNA 3'-end processing
DDX43	ATP-dependent 3' 5' DNA helicase
DDX51	rRNA processing
DHX8	Spliceosomal complex disassembly
DNMT1	DNA methylation
EEF2K	Myosin filament disassembly
EIF2AK2	Translational initiation
EIF2AK4	Translational initiation
EIF4G2	Translational initiation
EIF5A	positive regulation of translational elongation
ER1	Exonucleolytic trimming involved in rRNA processing
FAM120C	tRNA
FAM98C	tRNA
GAR1	snoRNA-guided rRNA pseudouridine synthesis
GTPBP10	Ribonucleoprotein complex biogenesis
INTS10	snRNA processing
MAEL	piRNA processing
MRPL52	Mitochondrial translation
MRPL53	Mitochondrial translation
MRPL9	Mitochondrial translation
MRPS5	Mitochondrial translation
MTIF2	Mitochondrial translational initiation
MTRF1	Mitochondrial translational termination
MYEF2	Myotube differentiation

Name	Function
NOVA2	Regulation of alternative mRNA splicing, via spliceosome
OAS3	Regulation of chemokine (C-X-C motif) ligand 9 production
PAPOLG	mRNA polyadenylation
RBMY1E	Positive regulation of mRNA splicing
RPUSD4	mitochondrial tRNA pseudouridine synthesis
PSMA2	proteasome-mediated ubiquitin-dependent protein catabolic process
PPIL4	protein peptidyl-prolyl isomerization
RNMT	RNA 5'-cap (guanine-N7)-methylation
RPL31	Cytoplasmic translation
RRP1	rRNA processing
SCAF4	Negative regulation of termination of DNA-templated transcription
SNRPD1	U2-type SMN spliceosome assembly
SRPR	SRP-dependent co-translational protein targeting to membrane
TAF15	mRNA stabilization
TLR7	Toll-like receptor 7 signaling pathway
TGS1	7-methylguanosine cap hypermethylation
TRA2A	Positive regulation of mRNA splicing
TRDMT1	Regulation of tRNA stability
TUBA1B	Cytoskeleton-dependent intracellular transport
U2AF1	mRNA splicing
UBAP2L	Positive regulation of stress granule assembly
XPO4	Positive regulation of protein export from the nucleus
XPO7	Protein export from the nucleus
ZCCHC2	Nucleic acid binding activity

Supplementary Figure 1.1: Example of Rafts selected, Library preparation, list of candidates identified.

A. Example of positive rafts and negative control collected from microarray at 10x magnification.
B. Dislodged rafts collected with a magnetized wand are placed into individual tubes for DNA extraction and barcoded targeted PCR1 of the sgRNA insert.
C. Agarose gel of Pool PCR2 product for three representative libraries, each containing six pooled microRafts. Gel extraction was used to isolate the product of interest (red box).
D. Table identifying 55 proteins obtained for both CRaft-ID as described previously (Wheeler et al., 2020) and MAGeCK (Li et al., 2014).

RNA processing plays a pivotal role in governing the cellular localization of CHMP7.

Of the 55 genes, we prioritized 23 candidates which have appeared at least twice in the screen and have roles in RNA splicing, implications in ALS biology and RNA export/transport. We utilized XPO1, as a positive control that is known to facilitate the active export of CHMP7 from the nucleus (Vietri et al., 2020). While the precise details of CHMP7 nuclear localization are still an active area of research in several cell types, it involves interactions with other proteins and cellular structures involved in nucleocytoplasmic compartmentalization (Vietri et al., 2020; Thaller et al., 2019; Baskerville et al., 2023). To confirm that knocking down candidate proteins results in CHMP7 nuclear localization, we depleted each target in HeLa cells using two small interfering RNAs (siRNAs). We observed over a 50% increase in CHMP7 nuclear localization compared to non-targeting control for 13 targets (Supplementary Figure 2A). Where antibodies were available, we confirmed a minimum of 80% protein reduction through western blot analysis (Supplementary Figure 2B and 2C). We focused on eight candidates (NOVA2, DDX43, TUBA1B, FAM120C, SNRPD1, DHX8, XPO4, XPO7) that had minimal or no change in CHMP7 protein levels, indicating that translocation of CHMP7 was not due to overall changes in CHMP7 expression (Supplementary Figure 2D). Three of these candidates, XPO7, XPO4, and DHX8, are export factors known to mediate the nuclear export of proteins and RNA (Aksu et al., 2018; Xu et al., 2021; Felisberto-Rodrigues et al., 2019). However, SmD1 exhibited the highest increase in CHMP7 nuclear localization, reaching 98% (Supplementary Figure 2A). SmD1 is a component of the Sm-class small nuclear ribonucleoproteins (snRNPs) and is critical for the assembly of U4 snRNP (Weber et al., 2010), and has no prior reported interactions with CHMP7. Following the confirmation of knockdown (KD) for DHX8, XPO7, and SmD1 by western blot

analysis (Figure 2B-D), we assessed CHMP7 cytoplasmic and nuclear intensity in HeLa cells. Immunofluorescence analysis of siRNA-treated HeLa cells stained for CHMP7 demonstrated heightened nuclear levels in comparison to cytoplasmic levels, signifying a notable increase in CHMP7 nuclear localization (Figure 2E-G). This observed shift strongly suggests that the depletion of our candidate RNA processing proteins significantly contributes to the modulation of CHMP7's subcellular distribution.

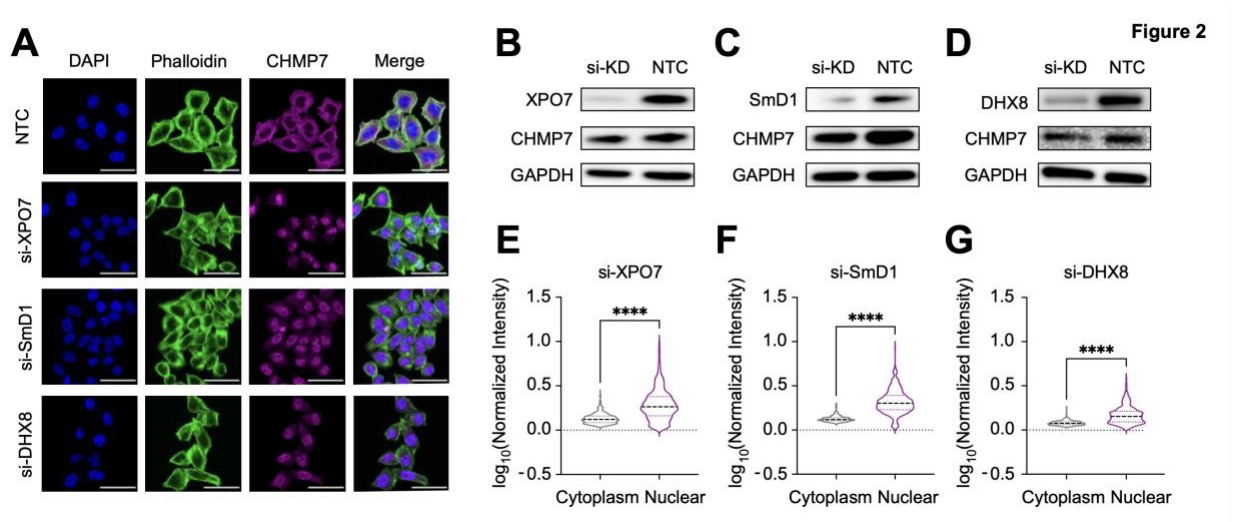

Figure 1.2: RNA processing plays a pivotal role in governing the cellular localization of CHMP7.

A. Representative images validation after protein depletion by siRNA of XPO7, DHX8, SmD1. HeLa cells stained with DAPI-Blue, Phalloidin (Actin filaments)-Green, CHMP7-Magenta. Scale bar, 50 μm.

B-D. Western blot validation of target protein depletion by siRNA of SmD1, DHX8, XPO7 alongside NTC.

E-G. Quantification of image intensity of cytoplasmic CHMP7 and nuclear CHMP7 in HeLa cells ± S.D. n = 3 wells. (4 images per well = total ~800 cells) normalized to NTC represents the y-axis as log10(normalized intensity). The data were presented as the mean ± SD of three independent experiments. The significance was analyzed by the student's t-test. ****$P < 0.0001$.

Supplementary Figure 1.2: siRNA validation of 23 candidates in HeLa cells.

A. siRNA depletion of target proteins in bulk cells with 2 siRNA per target. CHMP7 Nuclear intensity /number of DAPI was normalized to NTC for each experiment. Proteins are organized by the RNA-life cycle. Cut off 50% implemented with targets that caused more than 50% of cells to have positively higher intensity of nuclear CHMP7 relative to NTC in 3 biological replicates data presented as the mean ± SEM.
B. Western Blot validation of top candidates via siRNA compared to NTC.
C. Confirmation of siRNA KD of 80% of target proteins (n=2).
D. Quantification of CHMP7 protein level with siRNA. N.S-not significant (n=2).

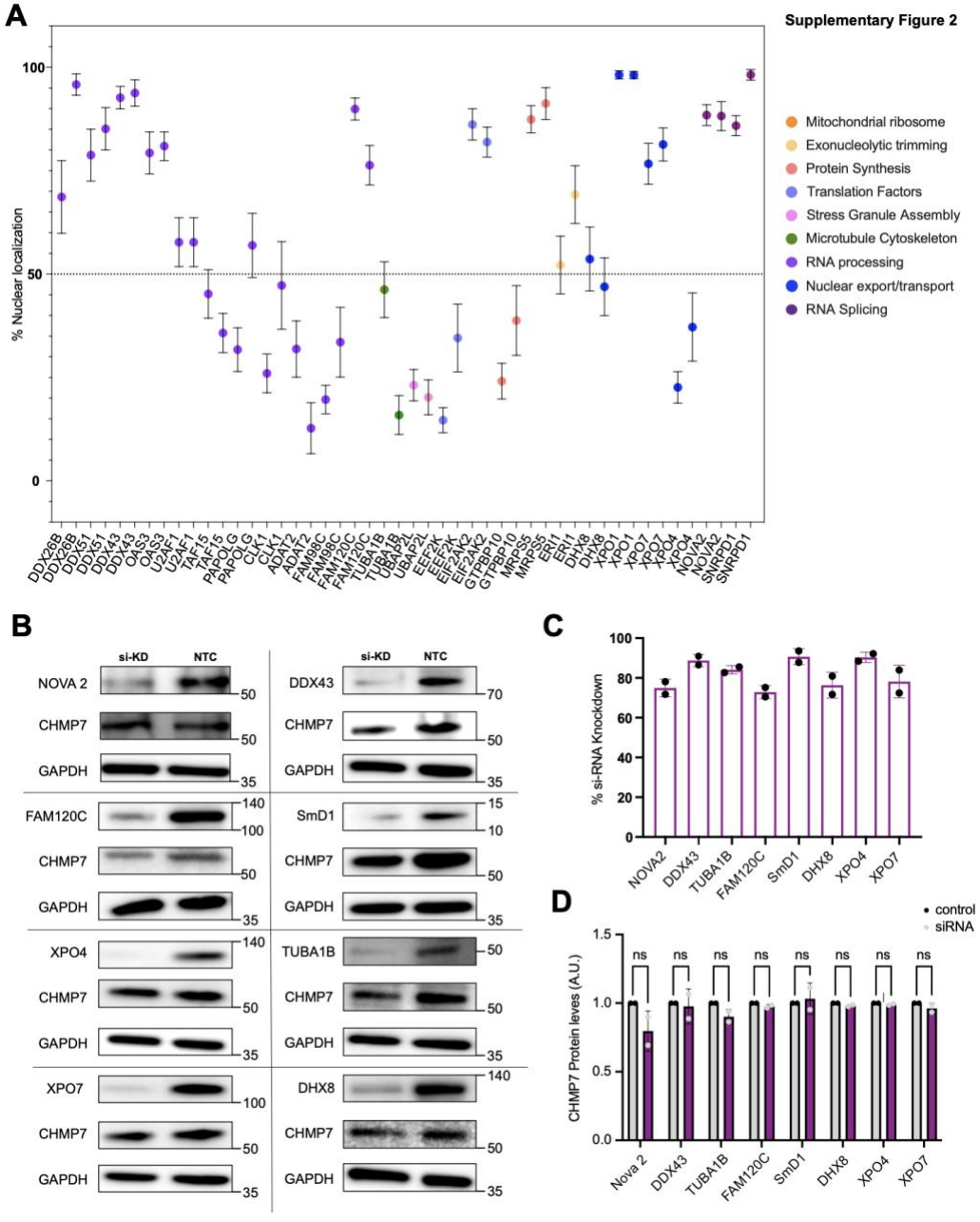

CHMP7 interacts with the SMN snRNP assembly complex.

To investigate whether CHMP7 interacts with our candidate proteins in an RNA-dependent manner, we immunoprecipitated (IP) endogenous CHMP7 protein complexes from iPSC-derived differentiated motor neurons at day 28 with or without RNase treatment, followed by mass spectrometry analysis (Figure 3A). We identified 379 enriched proteins in CHMP7-IP samples relative to an IgG control in the untreated condition (p-value<0.01 and greater than 2-fold difference; Figure 3B). CRaft-ID candidates SNRPD1/SmD1, EIF2AK2, RRP1, and GAR1 were identified as interactors of CHMP7 in the untreated samples, with two additional candidates EIF4G2 and XPO7 found as enriched under a less stringent p-value cutoff of 0.05 (Figure 3B). Following treatment with RNase, we observed an 75% reduction in the total number of enriched interactions, suggesting that CHMP7's protein-protein interactome is largely RNA-mediated (Figure 3C). In untreated conditions, the interacting proteins displayed an enrichment for RNA processing factors, such as RNA transport, splicing modulators, translation regulatory proteins, snRNPs, and RNA helicases (Figure 3D). In RNase-treated samples, this network shifted towards the SUMOylation of DNA methylation, glycogen synthesis and degradation, actin cytoskeleton organization, and glycogen metabolic process unrelated to RNA metabolism (Figure 3E). Despite CHMP7 being predominantly cytoplasmic, we identified both cytoplasmic and nuclear proteins, as well as those known to shuttle between the nucleus and cytoplasm, suggesting a functional role for CHMP7 in both cellular compartments consistent with prior reports (Chu et al., 2023; Webster et al., 2014; Webster et al., 2016; Gu et al., 2017; Olmos et al., 2016). We further performed cluster analysis to characterize molecular functions for the CHMP7 interacting proteins in untreated samples. Our analysis identified several candidates within the SMN complex, which itself is critical for biogenesis of spliceosomal snRNPs (Liu and Dreyfuss, 1996; Massenet et al., 2002), as well as within mRNA transport and RNA processing

machineries (Figure 3F). Upon closer examination of CHMP7 RNA-mediated interactions, we observed its close association with Gemin proteins and SmD proteins, all integral components of the snRNP assembly pathway (Figure 3G). Indeed, our analysis revealed a larger number of interactions with the components of the SMN complex compared to Nups (Figure 3G). Given that the biogenesis of spliceosomal snRNPs involves multiple steps in both nuclear and cytoplasmic phases, our results suggest that CHMP7 and SMN could be involved in a coordinated regulation of these RNA-related processes.

Figure 1.3: CHMP7 interacts with SMN complex proteins responsible for snRNP assembly in motor neurons.

A. Schematic of IP-MS workflow to identify CHMP7 protein-protein interactions with/without RNase treatment.

B-C. Proteins significantly enriched in CHMP7 IPs compared to RNase treatment matched IgG IPs. Volcano plots showing the log2 of the fold change (x-axis) vs the -log10 of p-values (unpaired Student's t-Test). All peptides and proteins were thresholded at a 1% false discovery rate (FDR). Proteins with p-values < 0.01 and FC > 2 are labeled as interactors.

D-E. The log10 of the p-value for the significance of enrichment is plotted for each GO term. Background of all the proteins in IPs was implemented in GO term analysis.

F. Complex network analysis was performed for CHMP7 interaction across all GO term pathways obtained with MCODE algorithm to find densely connected protein neighborhoods in the network. The biological roles of each component are annotated.

G. RNA-mediated interaction network for CHMP7 interactors snRNP assembly proteins (SMD1-3), GEM, and nuclear pore complex proteins. Nodes are colored based on k-means clustering and edge confidence; high (0.700), highest (0.900), medium (0.400) from String.

Figure 3

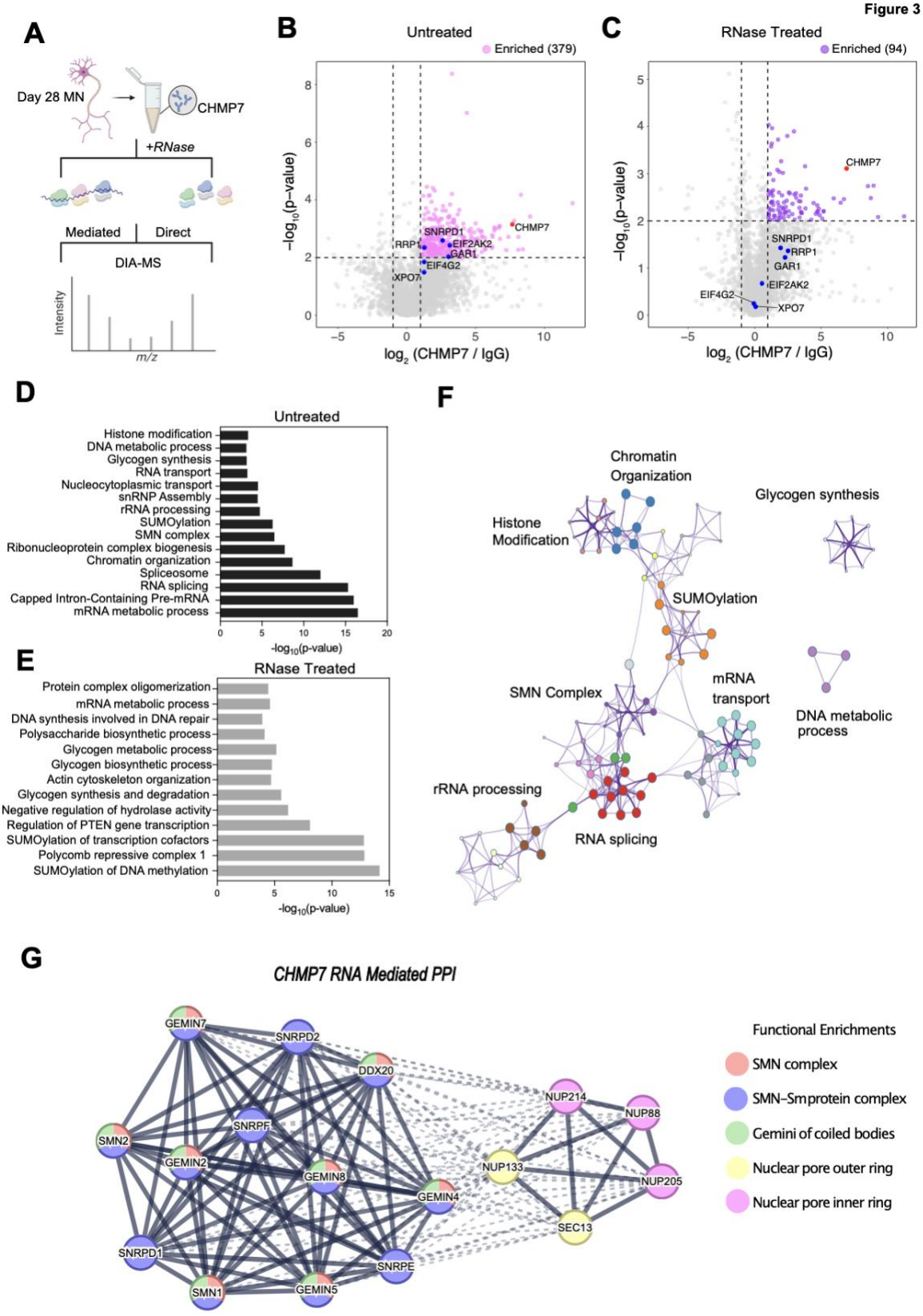
A
Day 28 MN
CHMP7
+RNase
Mediated
Direct
DIA-MS
Intensity
m/z
B
Untreated
Enriched (379)
−log10(p−value)
log2 (CHMP7 / IgG)
CHMP7
SNRPD1
RRP1
EIF2AK2
GAR1
EIF4G2
XPO7
C
RNase Treated
Enriched (94)
−log10(p−value)
log2 (CHMP7 / IgG)
CHMP7
SNRPD1
RRP1
GAR1
EIF2AK2
EIF4G2
XPO7
D
Untreated
Histone modification
DNA metabolic process
Glycogen synthesis
RNA transport
Nucleocytoplasmic transport
snRNP Assembly
rRNA processing
SUMOylation
SMN complex
Ribonucleoprotein complex biogenesis
Chromatin organization
Spliceosome
RNA splicing
Capped Intron-Containing Pre-mRNA
mRNA metabolic process
-log10(p-value)
E
RNase Treated
Protein complex oligomerization
mRNA metabolic process
DNA synthesis involved in DNA repair
Polysaccharide biosynthetic process
Glycogen metabolic process
Glycogen biosynthetic process
Actin cytoskeleton organization
Glycogen synthesis and degradation
Negative regulation of hydrolase activity
Regulation of PTEN gene transcription
SUMOylation of transcription cofactors
Polycomb repressive complex 1
SUMOylation of DNA methylation
-log10(p-value)
F
Chromatin Organization
Histone Modification
Glycogen synthesis
SUMOylation
SMN Complex
mRNA transport
DNA metabolic process
rRNA processing
RNA splicing
G
CHMP7 RNA Mediated PPI
GEMIN7
SNRPD2
DDX20
SNRPF
SMN2
GEMIN2
GEMIN8
GEMIN4
SNRPD1
SMN1
GEMIN5
SNRPE
NUP214
NUP88
NUP133
NUP205
SEC13
Functional Enrichments
SMN complex
SMN–Smprotein complex
Gemini of coiled bodies
Nuclear pore outer ring
Nuclear pore inner ring

CHMP7 binds to snRNAs and mRNA of splicing factors in human iPSC-motor neurons.

Given that 57% of CHMP7's interacting proteins are annotated RBPs, we reasoned that CHMP7 itself has RNA-binding capabilities. We employed the deep-learning RBP classifier HydRA (Jin et al., 2023) to identify potential RNA-binding associated domains (RBD) and low-complexity regions (LCRs) across the CHMP7 protein sequence. HydRA's occlusion map analysis indicates that CHMP7 has predicted RNA binding regions at 126-174 and 206-226 amino acids (AAs) ($p<0.05$), and at 141-166 AAs ($p<0.001$), proximal to the N-terminal of the Snf7 domain (Figure 4A). We conducted enhanced crosslinking and immunoprecipitation (eCLIP) analysis on CHMP7 in iPSC-MNs(Van Nostrand et al., 2016; Supplementary Figure 3A). Both CHMP7 IP replicates passed statistical thresholds to maximize the number of hits (Supplementary Figure 3B) as specified by the SKIPPER workflow (Boyle et al., 2023), and had high concordance between replicates (Supplementary Figure 3C). After processing all IPs separately, we selected reproducibly enriched windows for both transcriptomic regions and repetitive elements, satisfying a 20% false discovery rate cutoff (Supplementary Figure 3D).We found that CHMP7 interacts with transcripts from protein-coding genes (Figure 4B), binding primarily to CDS and 5' untranslated regions (5'UTR) (Figure 4C), suggesting that CHMP7 interacts with mature mRNAs in the cytoplasm, reminiscent of other RBPs that had CDS preferences analyzed by ENCODE3 (Van Nostrand et al., 2020) (Figure 4D). We assessed the motifs enriched within CHMP7 enriched regions and found two statistically significant motifs, namely CGG ($p<10^{-53}$) and UGG ($p<10^{-44}$) Supplementary Figure 3E).

To characterize the genes enriched for CHMP7 binding, we conducted a Gene Ontology (GO) enrichment analysis, revealing significantly enriched terms "axon extension," "transport along microtubule," "synapse assembly," "Splicesomal complex," "U2 and U5 SNRNP," and

"Dynein complex binding" (Figure 4E). To illustrate, we discovered CHMP7 binding to exonic regions of mRNAs encoding splicing factors SF1 and PRPF40 (Supplementary Figure 3F). These genes encode integral protein constituents of snRNPs or are actively engaged in alternative splicing through U1 or U2 (Makarov et al., 2012). We also observed binding to SNRNP70 which enables U1 snRNA binding activity (Supplementary Figure 3F). CHMP7 also exhibited enriched binding to noncoding RNAs such as miRNA, lncRNA and snRNAs such as RNU1, RNU2, and RN7SK (Figures 4B, 4F and 4G). This direct binding establishes connections to snRNA complex formation or regulation at the RNA level, complementing our protein-protein interaction results. In summary, CHMP7 appears to interact with the RNAs of splicing factors and snRNAs involved in snRNP formation and splicing.

Figure 1.4: CHMP7 binds RNA, specifically RNA processing targets.

A. Hydra analysis of CHMP7 RNA binding, CHMP7 Q8WUX9 IDR coordinates: 1-23, 224-225, 256-257, 261-263, 266-270, 293-293, 296-296, 347-376. Low complexity coordinates: 12-21, 33-33, 67-69, 149-159, 180-180, 209-2089, 251-251, 253-254, 256-258, 260-281, 284-285, 287-287, 382-384, 386-392, sig peak regions ($p<0.05$): 126-174, 206-226, sig peak regions ($p<0.001$): 141-166.
B. Pie chart of all enriched windows feature types.
C. Fold change in binding enrichment of CHMP7 after normalization to input in Day 28 motor neurons. SKIPPER analysis was performed to achieve binding enrichment across all IPs (Boyle et al., 2023).
D. Comparison of CHMP7 eCLIP to ENCODE3 eCLIP data. The clustering is based on binding preferences to transcript types, feature types, and repetitive elements.
E. Significant Skipper Gene Ontology enrichments for CHMP7 filled by log10 enrichment. The top cellular component, biological process, and molecular function term.
F. Heatmap indicates the relative information for 17 elements and CHMP7 enriched binding with one entry meeting a 0.5 relative information cutoff.
G. Example of snRNAs, (e.g. RNU2), related transcript non-coding binding between CHMP7 (dark gray) and matching input (gray). Similar pattern of binding among the two IPs.

Figure 4

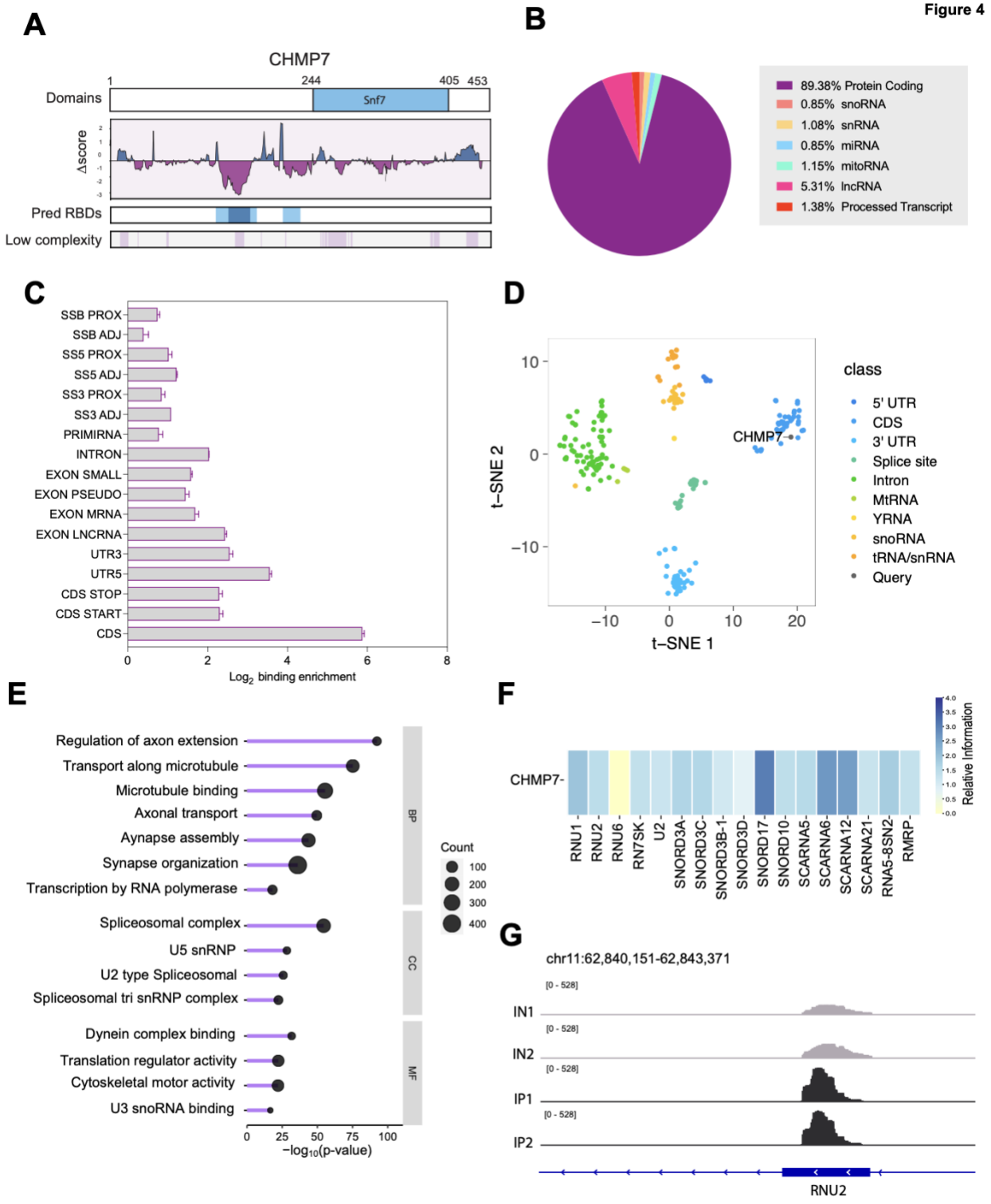
A
CHMP7
1
244
405
453
Domains
Snf7
Δscore
Pred RBDs
Low complexity
B
89.38% Protein Coding
0.85% snoRNA
1.08% snRNA
0.85% miRNA
1.15% mitoRNA
5.31% lncRNA
1.38% Processed Transcript
C
SSB PROX
SSB ADJ
SS5 PROX
SS5 ADJ
SS3 PROX
SS3 ADJ
PRIMIRNA
INTRON
EXON SMALL
EXON PSEUDO
EXON MRNA
EXON LNCRNA
UTR3
UTR5
CDS STOP
CDS START
CDS
Log2 binding enrichment
D
t–SNE 2
t–SNE 1
CHMP7
class
5' UTR
CDS
3' UTR
Splice site
Intron
MtRNA
YRNA
snoRNA
tRNA/snRNA
Query
E
Regulation of axon extension
Transport along microtubule
Microtubule binding
Axonal transport
Aynapse assembly
Synapse organization
Transcription by RNA polymerase
Spliceosomal complex
U5 snRNP
U2 type Spliceosomal
Spliceosomal tri snRNP complex
Dynein complex binding
Translation regulator activity
Cytoskeletal motor activity
U3 snoRNA binding
BP
CC
MF
Count
−log10(p-value)
F
CHMP7-
RNU1
RNU2
RNU6
RN7SK
U2
SNORD3A
SNORD3C
SNORD3B-1
SNORD3D
SNORD17
SNORD10
SCARNA5
SCARNA6
SCARNA12
SCARNA21
RNA5-8SN2
RMRP
Relative Information
G
chr11:62,840,151-62,843,371
IN1
IN2
IP1
IP2
RNU2

Supplementary Figure 1.3: CHMP7 quality control eCLIP analysis.

A. Antibody validation after cross-link and IP of CHMP7 in motor neurons with IgG control obtained from Jess Simple Western System.
B. Threshold scan produced by SKIPPER pipeline of two-IPs.
C. Concordance between replicates.
D. Number of enriched windows and tested windows.
E. HOMER top significant CHMP7 RNA binding motifs.
F. IGV track of SNRNP70, SF1, PRPF40 with two inputs and two IPs.

Supplementary Figure 3

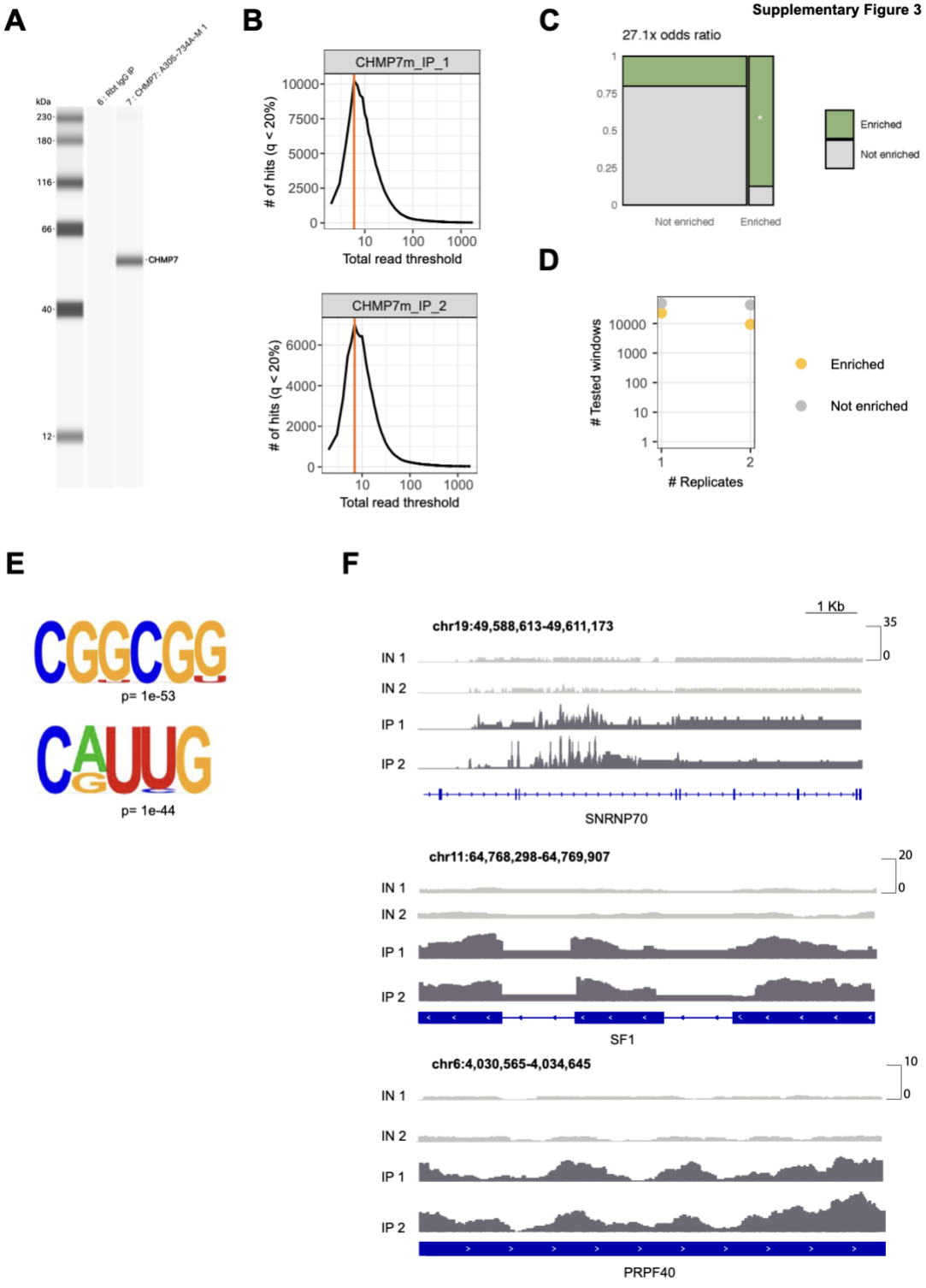

ACKNOWLEDGEMENTS

I would like to acknowledge Professor Gene Yeo for their support as the chair of my committee. Through multiple drafts and many long nights, their guidance has proved to be invaluable.

Chapter 1 , in full, is a reprint of the material as is in production at Neuron. To, J., Gautam, V., Naritomi, J., Nguyen, C., Lee, B., Lam, D., Avina, A., Mizrahi, O., Yeo, G. W. (2024) .Inhibition of RNA splicing triggers CHMP7 nuclear entry, impacting TDP-43 function and leading to the onset of ALS. Accepted at Neuron. The dissertation author was the primary investigator and author of this paper.

Chapter 2 Inhibition of RNA splicing triggers CHMP7 nuclear entry leading to onset of ALS

Abnormal nuclear accumulation of CHMP7 can initiate NPC injury and cause defects in NCT, resulting in TDP-43 dysfunction and mislocalization in human ALS neurons (Coyne et al., 2021). Recent studies have demonstrated that SUN1 mediated alterations to NPC permeability barrier integrity facilitate increased nuclear influx of CHMP7 in sALS iPSNs (Baskerville et al., 2023). However, the mechanisms and molecular players underlying regulation of CHMP7 subcellular distribution remain unknown and are of critical importance to our understanding of early pathogenesis of ALS.

Here, we employed high-throughput imaging-based custom RNA binding protein-focused CRISPR/Cas9-based knockout screening technologies utilizing microRaft arrays to identify molecular regulators of CHMP7 nuclear localization. This screening approach identified 55 novel candidates influencing the subcellular distribution of CHMP7, many of which have been previously implicated in RNA processing, translation, and splicing regulation. Our subsequent investigations focused on the validation of 23 identified candidates, selected based on their potential relevance to ALS pathogenesis and roles in RNA processing. These validation experiments revealed that depletion of specific RNA processing proteins, including export factors, helicases, and splicing proteins, led to a substantial increase in CHMP7 nuclear localization. Notably, SNRPD1/SmD1 emerged as a primary candidate in controlling CHMP7's subcellular localization, showcasing one pathway which can influence CHMP7 translocation specifically.

To explore the RNA-binding capabilities of CHMP7, we conducted a transcriptome-wide analysis of its RNA substrates. Our findings revealed CHMP7's affinity for both snRNAs (RNU1 and RNU2) and RNAs that encode for protein-coding genes, particularly in exonic

regions and the 5'UTR (Figure 1.4C, 1.4F-G). Although we did not observe direct binding of CHMP7 to SmD1, we confirmed its interaction with snRNAs, specifically RNU1 and RNU2, which are components of the U1 spliceosome. Interestingly, when CHMP7 abnormally localizes to the nucleus in ALS iPSC-MNs, its binding profile shifts to intronic regions, suggesting an interaction with pre-RNA likely due to its nuclear localization. Our discovery further underscores the notion of pathway-level dysregulation in cellular RNA splicing processes as a link to the progression in the context of ALS as previously have been reported (Lehmkuhl and Zarnescu, 2018; Xue et al., 2020).

Impaired nuclear export of CHMP7 has consequences on RNA processing.

To investigate the potential impact of CHMP7's subcellular localization on RNA metabolism, we obtained two mutants of CHMP7 from a previous study done on nuclear envelope reformation and modified the plasmids with EF-1α promoter (Gatta et al., 2021). Predictions suggested that two nuclear export sequences (NESs) in Helices 5 and 6 (Vietri et al., 2020; Thaller et al., 2019) regulate CHMP7's interaction with XPO1. To generate nuclear localized CHMP7 cell models, we depleted CHMP7 in HeLa cells using siRNAs and transfected GFP-tagged CHMP7 mutants: GFP-CHMP7, GFP-CHMP7-Helix6, and GFP-CHMP7-Helix5-Helix6. As anticipated, while observing nuclear accumulation of CHMP7 with the Helix6 mutant, the Helix5-Helix6 mutant demonstrated clustering at the nuclear envelope and peripheral ER instead as previously shown before (Figure 1A) (Gatta et al., 2021). We next performed RNA-seq analysis on cells transfected with GFP-CHMP7-Helix6 relative to control GFP-CHMP7 to identify genes that are differentially expressed because of CHMP7 localization (Figure 1B). GO analysis of genes downregulated by CHMP7 nuclear localization were enriched for cytoplasmic translation, RNA splicing, mitochondrial translation, spliceosomal complex

assembly, and nuclear export. Upregulated genes were involved in metabolic processing (Figure 1C). Using rMATS turbo v4.1.2, we also identified a total of 1123 alternative splicing (AS) events with an FDR ≤ 0.05 between GFP-CHMP7-Helix6 vs GFP-CHMP7, of which 529 events exhibited a change in percent-spliced-in (Ψ) value of 10% or more (Figure1 D). An analysis of the genes with AS events highlighted "mRNA splicing" and "chromatin organization" as the most highly represented GO terms (Supplementary Figure 1A). This indicates that nuclear retained CHMP7 impacts crucial cellular processes related to RNA metabolism.

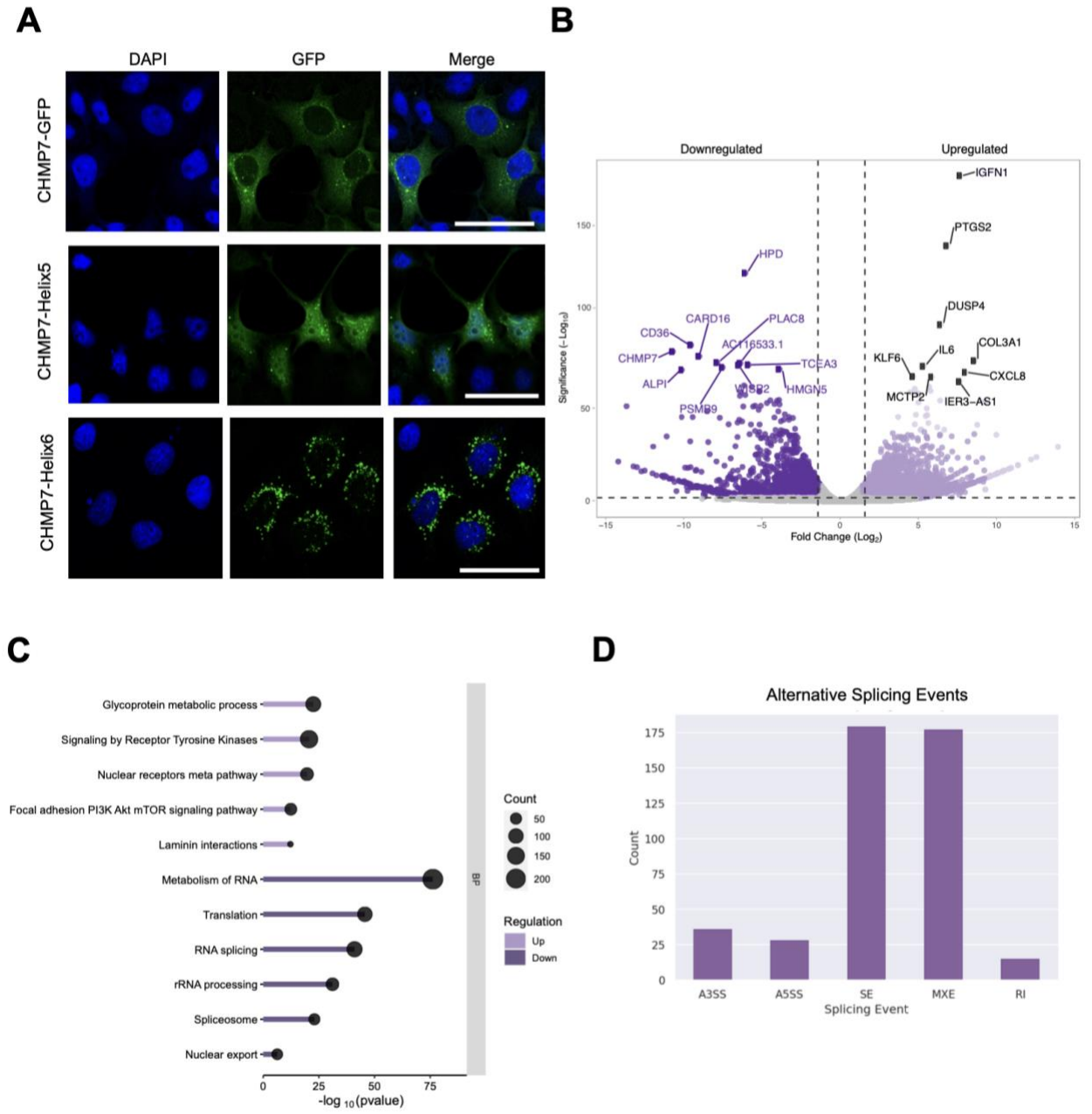

Figure 2.1: Downregulation of RNA processing upon CHMP7 nuclear accumulation in HeLa cells.

A. Immunofluorescence staining of GFP-CHMP7, GFP-CHMP7-helix6, GFP-CHMP7- helix5-helix6 stained with DAPI in HeLa Cells. Scale bar, 50 μm.
B. Volcano plot of GFP-CHMP7-Helix6 vs GFP-CHMP7. The p-value threshold of 0.05 and a FC of 2 as a cutoff.
C. Gene Ontology of downregulated and upregulated transcripts.
D. Distribution of the number of alternative splicing events identified across each AS event type filtered by FDR≤0.05+|ΔΨ|<0.1 (FDR) and FDR≤0.05+|ΔΨ|≥0.1 (FDR+PSI).

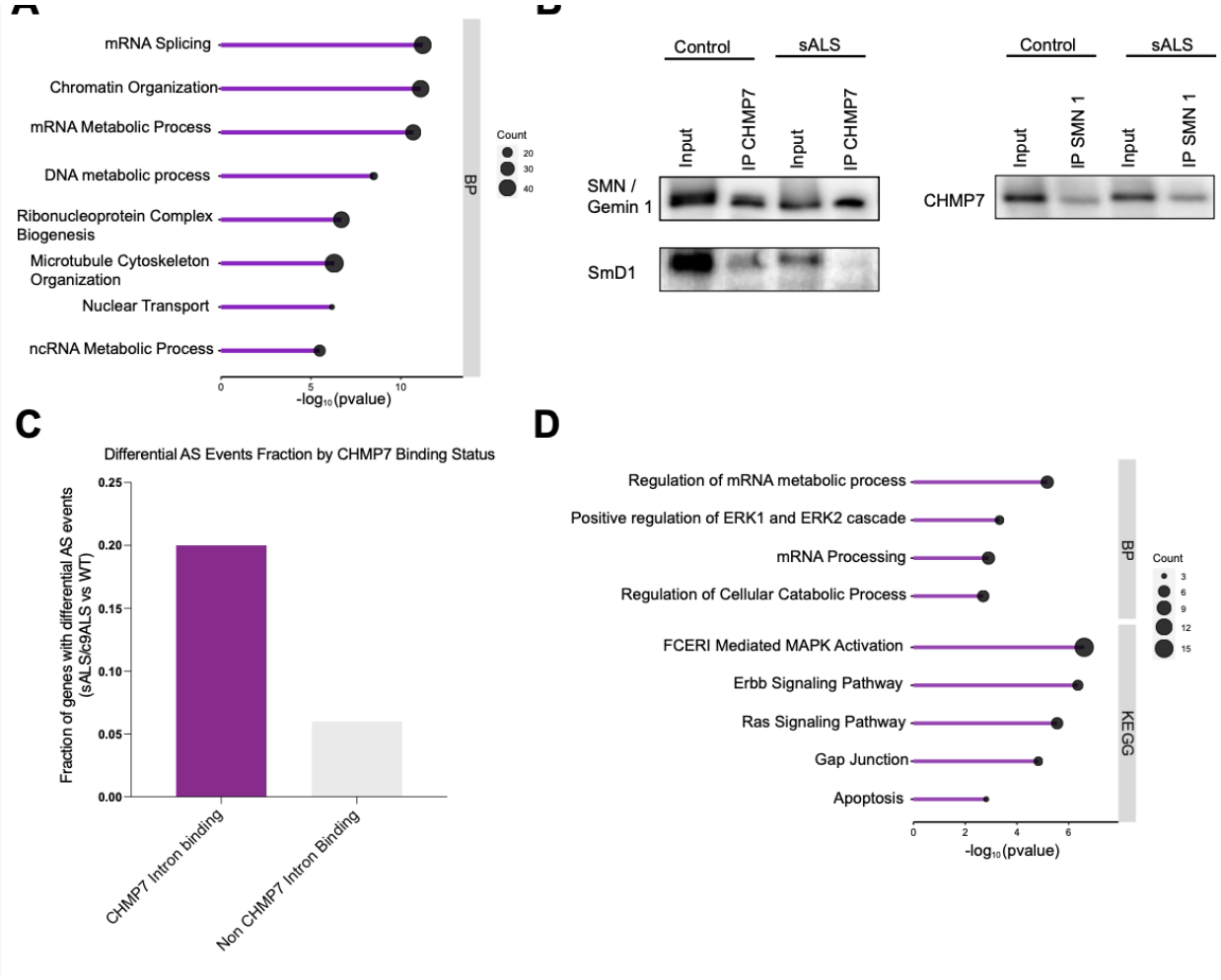

Supplementary Figure 2.1: Nuclear CHMP7 protein and RNA landscape profiling.
A. Metascape analysis and top GO terms associated with the aggregated genes having AS events in GFP-CHMP7-Helix6.
B. co-IP of CHMP7, SMN, and SmD1 in control and sALS.
C. Fraction of genes that contained alternatively spliced exons between sALS/C9orf72 versus control.
D. Metascape analysis and top GO terms associated with the aggregated genes having CHMP7 intron binding in sALS/c9orf72 ALS.

Changes in both RNA binding profile and protein interactions in sALS iPSC models.

Next, we investigated whether there are differences in the protein interactors of CHMP7 in iPSC-derived differentiated motor neurons (MNs) from sALS lines. We performed the IP of CHMP7 and evaluated it for interacting SMN-complex proteins by western blot analysis. We observed a slight reduction in SmD1 interaction with CHMP7 in sALS lines (Supplementary Figure 1B). This observation led us to exploring transcriptome-wide CHMP7 protein-RNA landscape in ALS iPSC models, where CHMP7 is aberrantly localized within the nucleus. To accomplish this, we generated MNs from iPSC lines from two healthy controls, two familial ALS patients with G4C2 repeat expansions in the C9ORF72 locus and two sALS patients. To identify CHMP7 RNA-binding in ALS, we conducted eCLIP analysis (Van Nostrand et al. 2016) on each cell line using an antibody recognizing endogenous CHMP7 protein, and quantified the number of enriched transcriptomic regions bound by the protein. In healthy control iPSC-MNs, we found a substantial enrichment in CDS and exons as we previously observed (Figure 2A, Figure 1.4C). However, in both C9orf72 and sALS iPSC-MNs, we discovered a threefold reduction in CHMP7 binding to CDS, coupled with an increase in binding to intronic regions (Figure 2B-C). Upon performing cluster analysis, we observed that CHMP7 binding in C9orf72 and sALS iPSC-MNs clustered with RBPs that typically interacted with intronic regions and splice sites (Figure 2D). By averaging across all transcripts using metadensity plots (Her et al., 2022), we detected prevalent intronic region binding, most likely due to its nuclear localization, by CHMP7 in both C9orf72 and sALS iPSC-MNs (Figure 2E). Concurrently, we saw a reduction in 5'UTR binding in sALS iPSC-MNs compared to control lines (Figure 2F). Next, we analyzed AS events from sALS and C9orf72 iPSC-MN compared to control RNA-seq datasets (Krach et al., 2022). At a FDR ≤ 0.01, we identified 1038 AS events that exhibited a change of Ψ of more

than 10% between ALS and control (Supplementary Figure 1C). We then tested the hypothesis that there was an association between CHMP7 binding and AS-containing genes. Out of 49 genes with intronic CHMP7 binding sites, 10 exhibited differential AS events. Among the 15,922 non-CHMP7-bound genes, 1,028 had significant events, confirming a statistically significant association ($p<0.00007$; chi-square statistic of 15.69; Supplementary Figure 1C). The 49 genes with enriched intronic binding were associated with GO terms "Regulation of mRNA metabolic process," "Positive regulation of ERK1 and ERK2 cascade," "Regulation of cellular catabolic process," "FCERI Mediated MAPK Activation," and "Apoptosis" (Supplementary Figure 1D). Our findings indicate that the abnormal nuclear localization of CHMP7 in C9orf72 and sALS iPSC-MNs contributes to its increased interactions within pre-mRNA intronic regions, likely affecting AS and other RNA processing events. Consequently, this aberrant localization leads to decreased interactions with mature mRNAs.

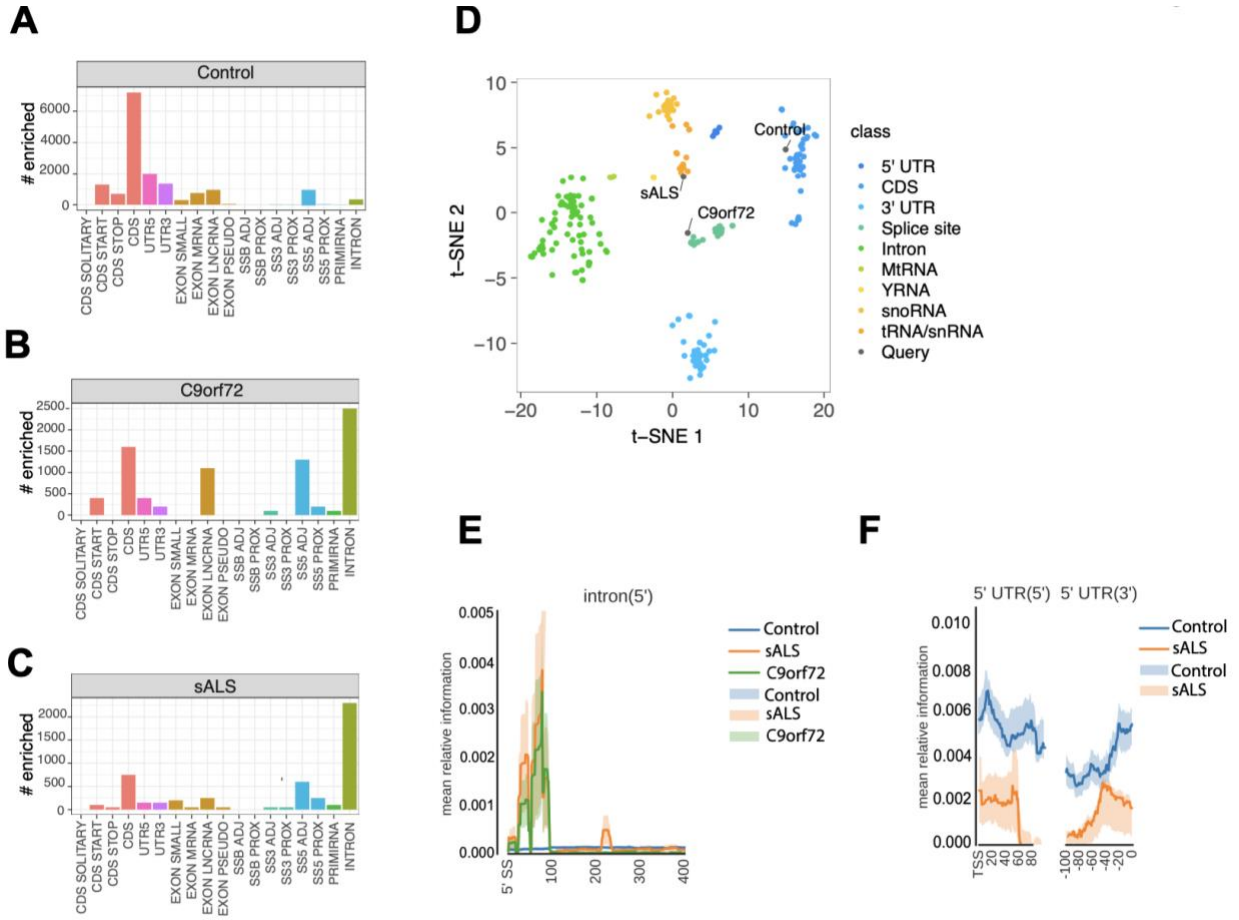

Figure 2.2: Alterations in CHMP7 protein and RNA landscape with a preference for RNA-binding PPI and increased intronic transcript binding in ALS.
A-C. Number of enriched windows across control, C9orf72, sALs.
D. Skipper t-SNE query of CHMP7 binding in across control, C9orf72, sALs against ENCODE eCLIP data colored by target preference.
E. Mean relative information around introns for CHMP7 control, C9orf72, and sALs in lines.
F. Mean relative information around 5'UTR for CHMP7 in control and sALs lines.

Overexpression of SmD1 is sufficient to restore subcellular distribution of CHMP7 in sALS iPSC models.

Our experiments demonstrated that depletion of SmD1 led to abnormal nuclear localization of CHMP7 in HeLa cells (Figure 1.2A, 1.2F). Previous studies have demonstrated that SmD1 depletion blocks splicing at the initial step, resulting in decreased levels of U1, U2, U4, and U5 (Mandelboim et al., 2003). Given these results, we investigated whether reducing SmD1 levels would induce CHMP7 nuclear localization. After nucleofection with SmD1-targeting siRNA in control iPSC-MNs, we observed increases in nuclear intensity of CHMP7 (Figure 3A-3B). It has been described that the increased nuclear localization of CHMP7 takes place as an early event in ALS, occurring prior to the manifestation of NPC injury (Coyne et al., 2020). Therefore, we determined whether SmD1 depletion could initiate NPC injury, presumably following CHMP7 nuclear localization in control iPSC-MNs. We observed reductions in POM121 and Nup133 upon SmD1 protein depletion (Supplementary Figure 2A-2B). We next quantified the nuclear intensity of TDP-43 and observed a reduction in TDP-43 immunoreactivity upon SmD1 knockdown compared to non-targeting-control (NTC) (Figure 3A, 3C). Therefore, we conclude that reduction of SmD1 in iPSC-MNs is sufficient to trigger NPC alterations that have previously been demonstrated to follow aberrant CHMP7 nuclear localization (Coyne et al., 2021).This overall loss of Nups is thought to impact nuclear transport, disrupt the function of Ran, and result in the loss of TDP-43 nuclear localization and aggregation in the cytoplasm (Chou et al., 2018; Rothstein et al., 2023).

To assess the functional consequences of altered TDP-43 distribution, we probed for changes in STMN2 cryptic exon splicing, which was recently found to be a prominent feature of ALS in patients with TDP-43 pathology (Jo et al., 2020; Klim et al., 2019; Melamed et al.,

2019). We performed quantitative reverse transcription polymerase chain reaction (RT-qPCR) analysis to quantify full-length and truncated STMN2 mRNA species in the context of SmD1 knockdown. Our findings revealed a reduction in the total abundance of full-length STMN2 mRNA, accompanied by a corresponding increase in truncated STMN2 mRNA (Supplementary Figure 2C-2D). Furthermore, to understand if SmD1 KD causes downstream consequences on motor neuron health, we observed glutamate-induced excitotoxicity with SmD1 KD in control iPSCs (Supplementary Figure 2F). Conversely, to investigate whether the restoration of SmD1 could influence STMN2 expression patterns, we demonstrate that overexpression of SmD1 led to the restoration of STMN2 levels while concurrently reducing truncated STMN2 mRNA abundance (Figure 3C-3D). Furthermore, we noted a substantial restoration of CHMP7 cytoplasmic localization following the increase in SmD1 levels, (Figure 3F-3G, Supplementary Figure 2E).

Prior proteomics work in sALS patient tissue depicted that SMN protein is reduced, in correlation with increased disease severity (Piao et al., 2011). This finding aligns with recent research conducted on sALS spinal cord tissues, where laser capture microdissection and proteomic analysis unveiled a striking decrease in the abundance of SMN core component SmD1 (Guise et al., 2023). Further supporting these observations, we observed a significant reduction of SmD1 mRNA levels in ALS (12 sALS and 8 C9ORF72) day 32 iPSC-MNs relative to controls (Figure 3H). We had also noticed a reduction of NOVA2 and TAF15 expression, but not DHX8 and XPO7 in these analyses (Supplementary Figure 3). Collectively, these data provide compelling evidence that the core small nuclear ribonucleoprotein particle splicing factor SmD1 plays a pivotal role in modulating the nuclear localization of CHMP7.

Figure 2.3: Overexpression of SmD1 can sufficiently rescue CHMP7 cytoplasmic levels in sALS.

A. Immunofluorescence of Day 28 IPSNs motor neurons with either NTC and SmD1 KD, stained with CHMP7 and TDP-43. Showing CHMP7 nuclear localization in SmD1 KD and reduction in nuclear TDP-43. Scale bars, 10 μm.
B. Quantification of nuclear and cytoplasmic ratio of CHMP7 intensity in motor neurons. Total of ~150 cells analyzed (n=3).
C. Quantification of nuclear TDP-43 levels with SmD1 KD compared to NTC total of ~50 cells analyzed (n=3).
D. mRNA levels for SmD1 were analyzed in 12 sALS lines and 8 C9orf72 and normalized to GAPDH and control samples.

E-F. Overexpression of scramble and SmD1 at day 32 in sALS lines, compared to control, showing mRNA levels for STMN2 and truncated STMN2 (n=5).

G. Immunofluorescence staining of neurons overexpressed with scramble and SmD1 constructs in sALS at day 36, following SmD1 construct overexpression for 4 days. Neurons were stained with CHMP7 (red), MAP2, and DAPI. Scale bars represent 10 μm.

H. Quantification of nuclear CHMP7 in neurons overexpressing SmD1 (n=3). The data are presented as the mean ± SD of three independent experiments. Significance was assessed using Student's t-test (*$p < 0.05$, ***$p < 0.001$, ****$p < 0.0001$).

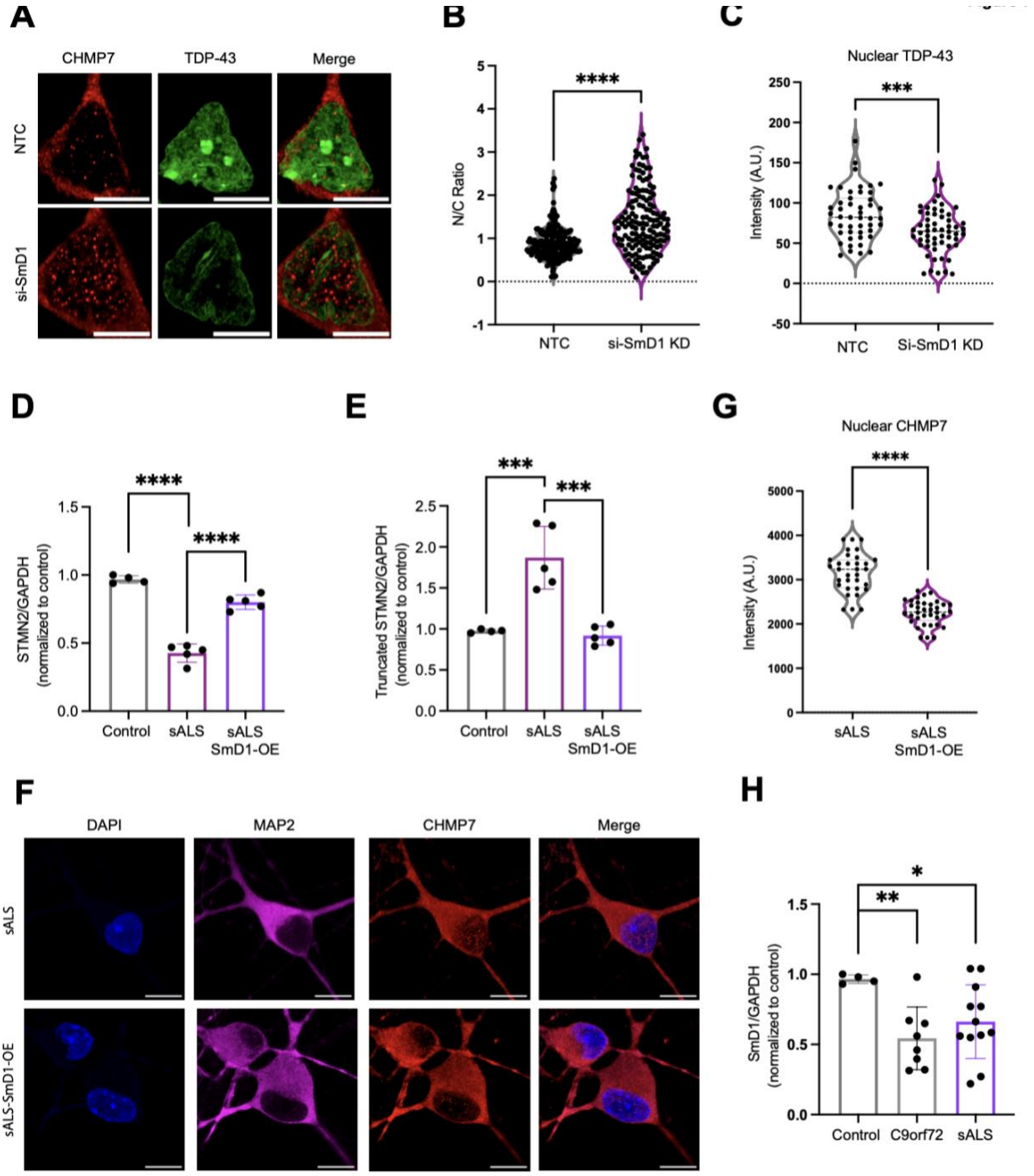
A
CHMP7
TDP-43
Merge
NTC
si-SmD1
B
N/C Ratio
****
NTC
si-SmD1 KD
C
Nuclear TDP-43
***
Intensity (A.U.)
NTC
Si-SmD1 KD
D
STMN2/GAPDH
(normalized to control)
****
****
Control
sALS
sALS
SmD1-OE
E
Truncated STMN2/GAPDH
(normalized to control)
***
***
Control
sALS
sALS
SmD1-OE
G
Nuclear CHMP7
****
Intensity (A.U.)
sALS
sALS
SmD1-OE
F
DAPI
MAP2
CHMP7
Merge
sALS
sALS-SmD1-OE
H
SmD1/GAPDH
(normalized to control)
*
**
Control
C9orf72
sALS

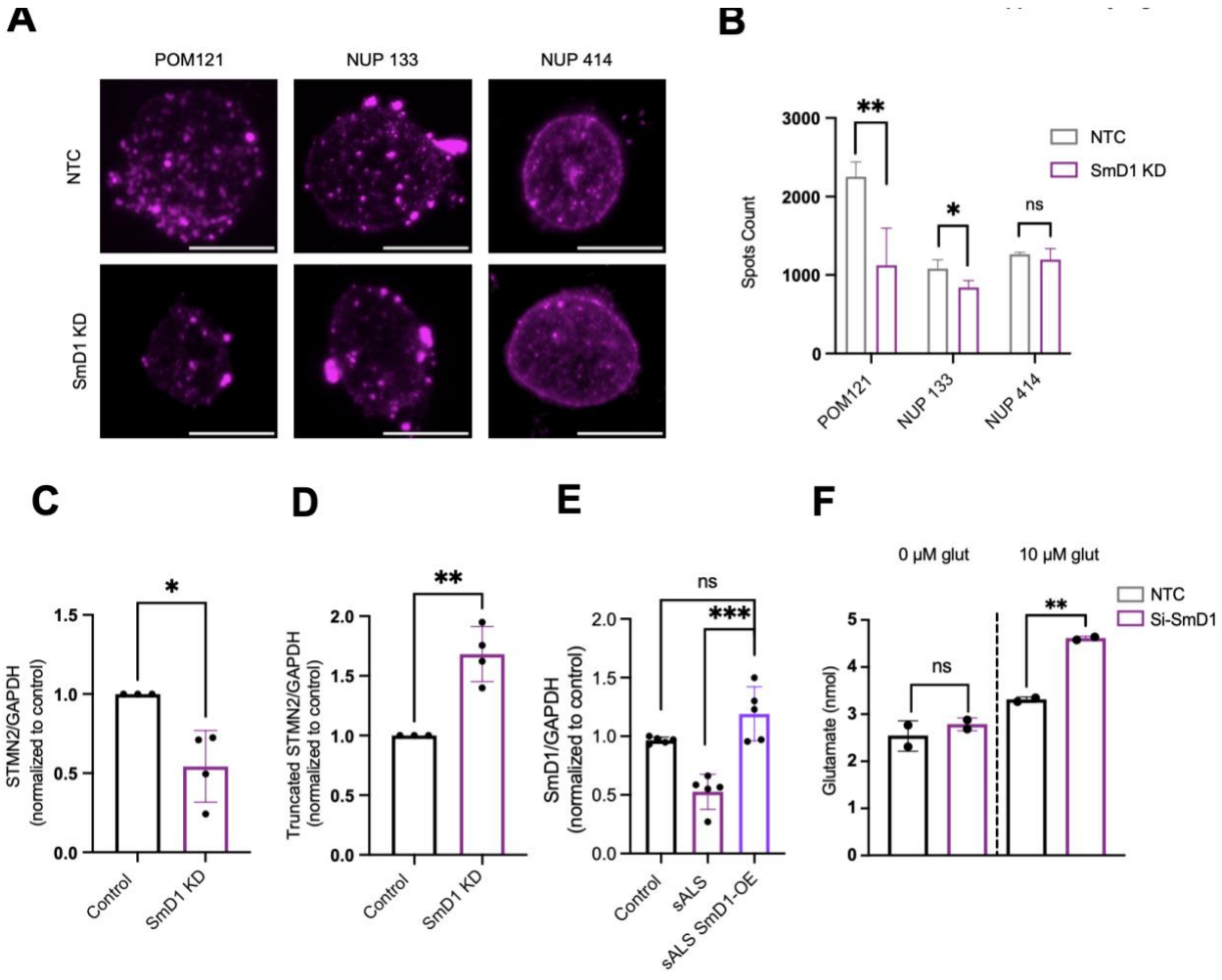

Supplementary Figure 2.2: Downregulation of SM supcore complex protein SmD1 initiates CHMP7 nuclear influx localization and alteration in NPC proteins.

A. Nuclei isolated from NTC and SmD1 KD. Stained with NPC proteins POM121, NUP133, NUP414.

B. Quantification of Nup spots of POM121, NUP 133, NUP414 (n=3).

C-D. qRT-PCR of STMN2 and truncated STMN2 in NTC and SmD1 KD. GAPDH was used for normalization (n=4).

E. mRNA levels for SmD1 were analyzed in sALS lines at day 32 in culture, normalized to GAPDH and control samples (n=5).

F. Quantification of nMol glutamate after exposure to (0 uM or 10uM) glutamate in control and SmD1 KD iPSNs (n = 2). The data were presented as the mean ± SD of different samples. The significance was analyzed by the student's t-test. * $p < 0.05$, **$P < 0.01$, ***$P < 0.001$.

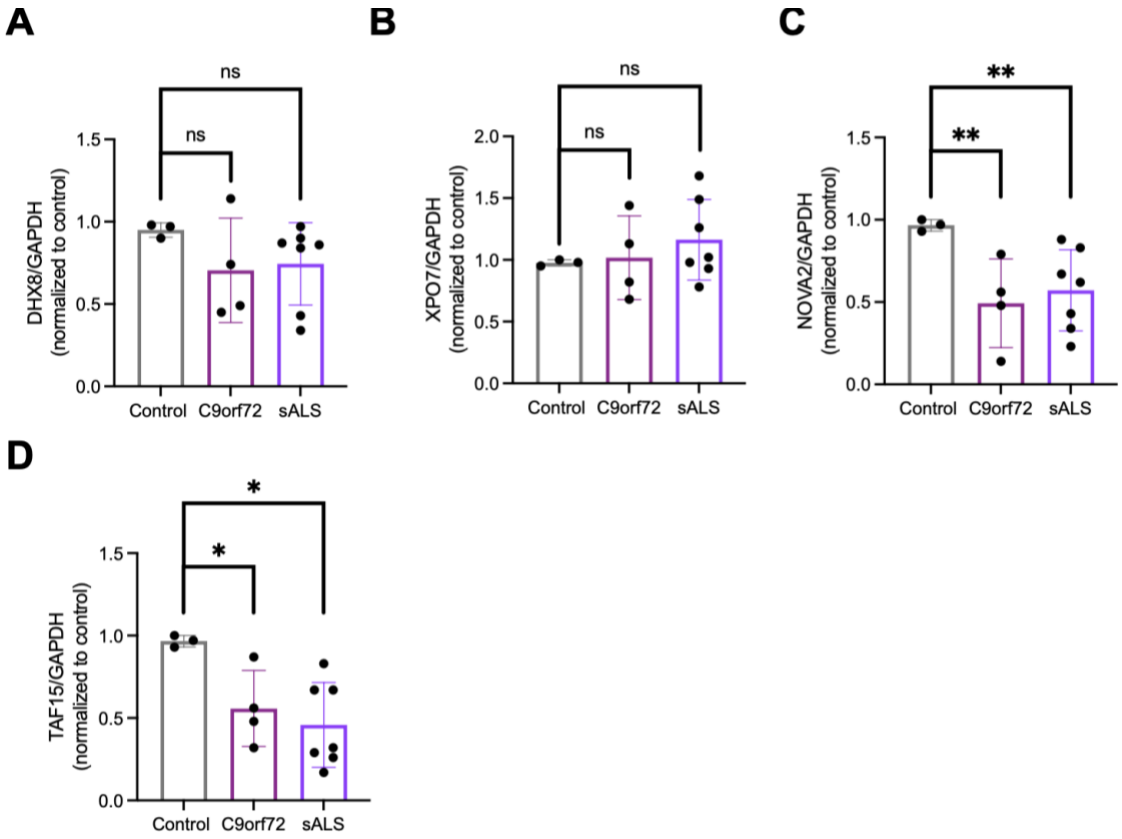

Supplementary Figure 2.3: Candidate transcript quantification in sALS and C9orf72 lines. A-D. qRT-PCR of DHX8, XPO7, NOVA2, TAF15 in 7 sALS lines and 4 C9orf72. GAPDH was used for normalization. The significance was analyzed by the student's t-test. ns-not significant * $p < 0.05$, **$P < 0.01$.

Pharmacological inhibition of snRNP assembly leads to CHMP7 nuclear localization.

As an alternative to the genetic depletion of SmD1 protein, we next determined whether pharmacological inhibition of snRNP assembly would alter nuclear/cytoplasmic translocation using live-cell imaging. Live-cell microscopy of GFP-CHMP7 and mCherry-TDP43 was conducted in HeLa cells subjected to either mock treatment or treatment with a commercially available SMN inhibitor at the same concentrations previously documented (2 hours at 200 μM; Liu et al., 2022). Intriguingly, GFP-CHMP7 rapidly localized to the nucleus following snRNP inhibition (Figure 4A-4B). Over a 2-hour treatment period, CHMP7 coalesced at the nuclear periphery, a phenomenon previously observed during the maintenance of nuclear envelope homeostasis during cell division (Stoten and Carlton, 2018; Gu et al., 2017; Von Appen et al., 2020). Endogenously, we performed the same experiment and observed a robust pattern of nuclear influx of CHMP7 (Figure 4C, Supplementary Figure 4A) and changes in NPC barrier function (Supplementary Figure 4B). As for TDP-43, we observed subtle changes in the nuclear abundance of TDP-43 over the 2-hour period, with no significant translocation evident (Figure 4A). However, after a 24-hour treatment with the SMN inhibitor at 30 μM, we began to observe endogenous TDP-43 translocating to the cytoplasm with IF (Supplementary Figure 4C-D). Our findings build upon previous research (Coyne et al., 2021), supporting the interpretation that cytoplasmic TDP-43 translocation follows the aberrant nuclear localization of CHMP7 and associated nuclear pore injury (Figure 4D).

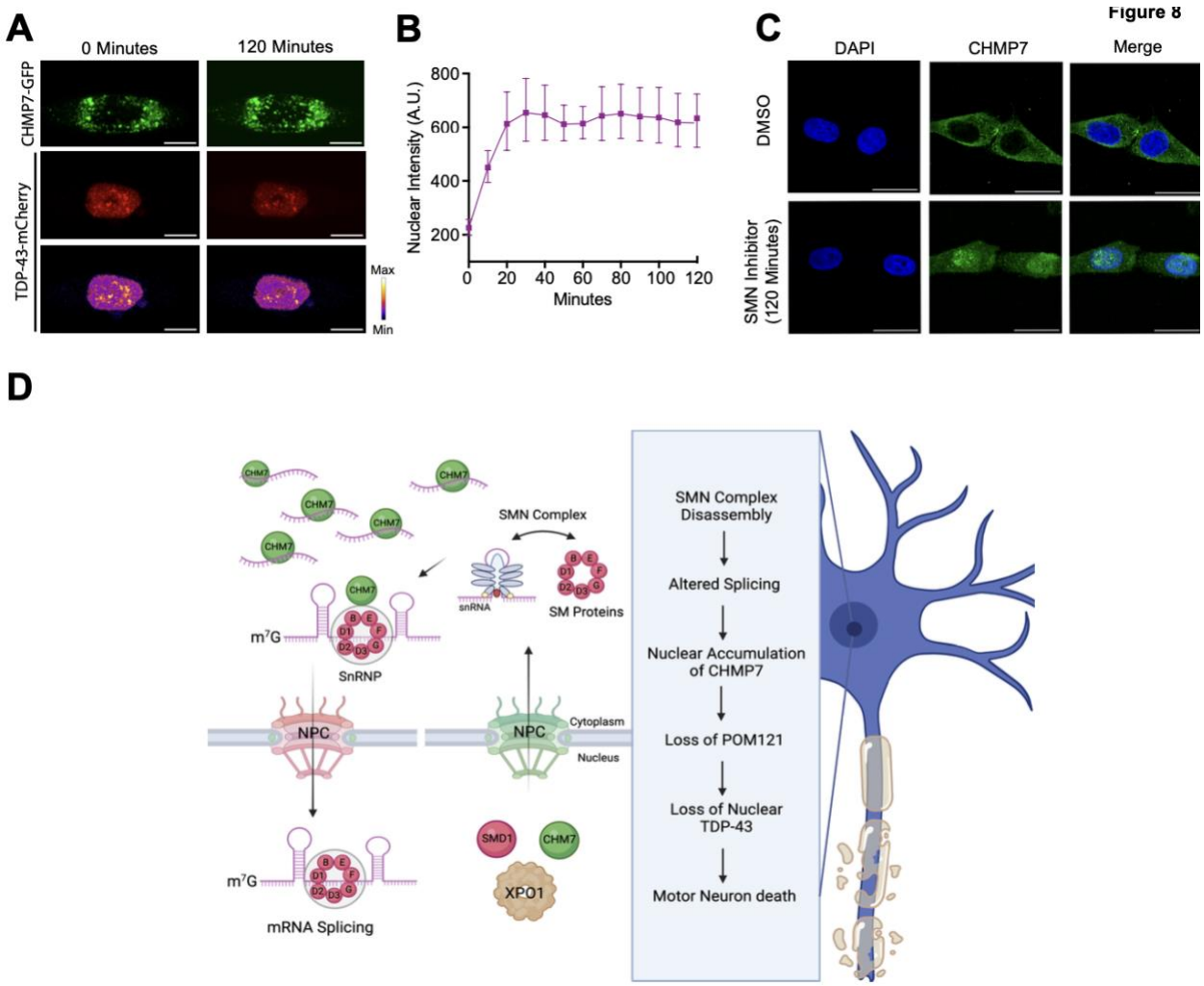

Figure 2.4: Perturbation of SMN-Complex-Dependent snRNP assembly modulates CHMP7 nuclear influx localization and alters NPC proteins.

A. Live cell imaging of GFP-CHMP7 and TDP-43-mCherry with treatment of SMN inhibitors at 0- and 120-minutes post SMN inhibitor treatment. Heatmap of fluorescent intensity ratio of TDP-43 at 0 min and at 120 min. Scale bars, 20 μm.
B. Time shows minutes (min); 0 min is just before SMN inhibitors. Error bars show ± SD. Nuclear GFP intensity, cells quantified, is ~12 used and averaged from three independent experiments.
C. IF staining of CHMP7 (Green) and DAPI with DMSO or SMN-inhibitor in HeLa after 2-hours (n = 3). Scale bars, 100 μm.
D. Proposed mechanism of action.

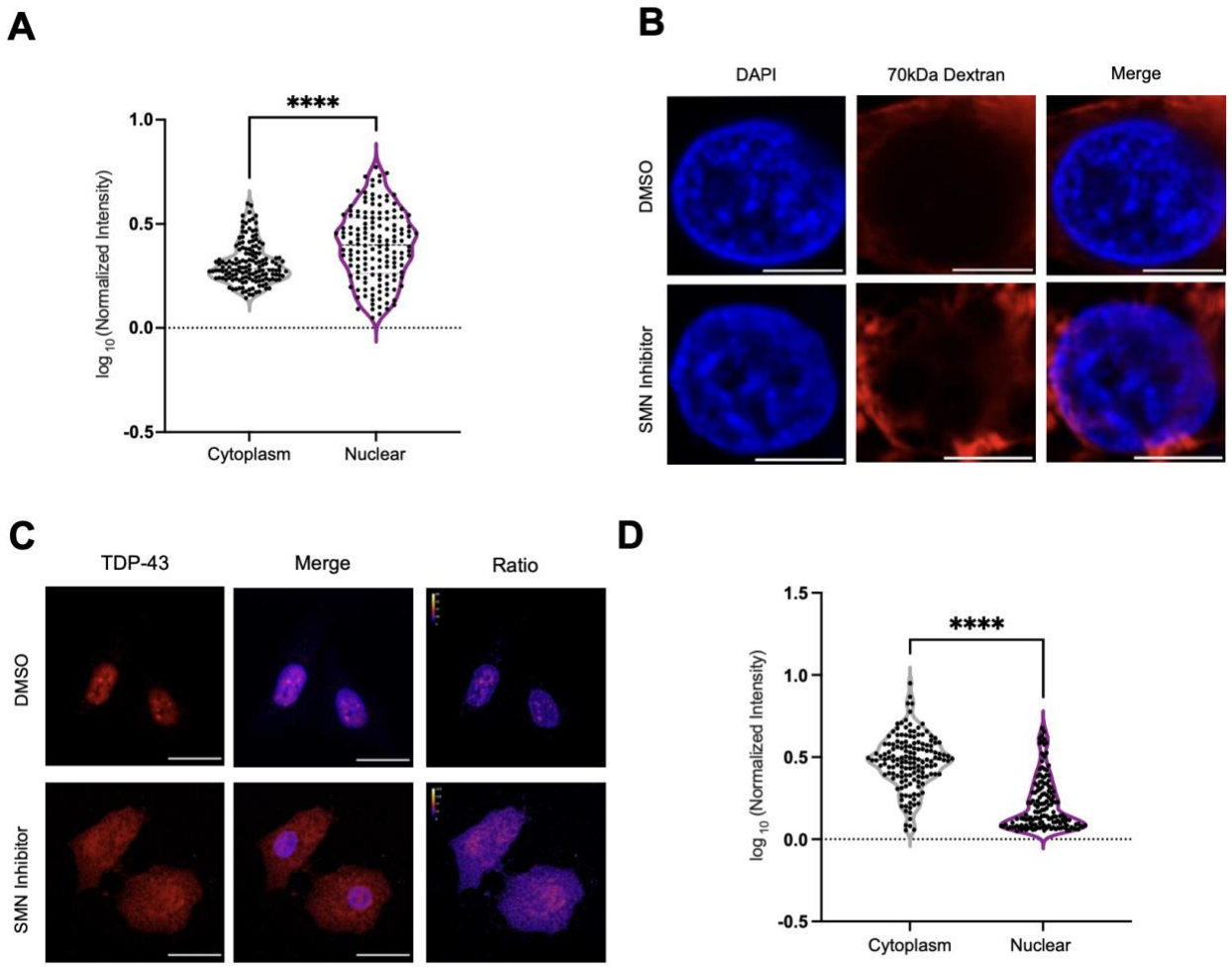

Supplementary Figure 2.4: Increased nuclear pore permeability with 24 hours SMN inhibition and downstream TDP-43 cytoplasm mislocalization in HeLa cells.

A. Quantification of cytoplasmic and nuclear CHMP7 image intensity in HeLa cells. Each data point represents the mean ± SD of three independent experiments, with n = 3 wells per experiment. Approximately 150 cells were analyzed in total (4 images per well). The y-axis displays log10(normalized intensity) relative to DMSO. Significance was determined using the student's t-test (****P < 0.0001).
B. Test of NPC barrier function in assembled nuclei. After treatment with a 30um SMN inhibitor and DMSO. Nuclei were isolated with a sucrose gradient and incubated with 70-kDa dextran (Red). Intranuclear 70-kDa dextran indicated leakiness of the nuclear membrane in treated cells. n = 3. Scale bars, 50 μm.
C. IF staining of TDP-43 (red) with DMSO or SMN-inhibitor in HeLa after 24- hours (n = 3). Scale bars, 100 μm.
D. Quantification of cytoplasmic and nuclear TDP-43 image intensity in HeLa cells. Each data point represents the mean ± SD of three independent experiments, with n = 3 wells per experiment. Approximately 150 cells were analyzed in total (4 images per well). The y-axis displays log10(normalized intensity) relative to DMSO. Significance was determined using the student's t-test (****P < 0.0001)

ACKNOWLEDGEMENTS

I would like to acknowledge Professor Gene Yeo for their support as the chair of my committee. Through multiple drafts and many long nights, their guidance has proved to be invaluable.

Chapter 2 , in full, is a reprint of the material as is in production at Neuron. To, J., Gautam, V., Naritomi, J., Nguyen, C., Lee, B., Lam, D., Avina, A., Mizrahi, O., Yeo, G. W. (2024) .Inhibition of RNA splicing triggers CHMP7 nuclear entry, impacting TDP-43 function and leading to the onset of ALS. Accepted at Neuron. The dissertation author was the primary investigator and author of this paper.

REFERENCES

Aksu, M., Pleiner, T., Karaca, S., Kappert, C., Dehne, H. J., Seibel, K., Urlaub, H., Bohnsack, M. T., & Görlich, D. (2018). Xpo7 is a broad-spectrum exportin and a nuclear import receptor. The Journal of cell biology, 217(7), 2329–2340.

An, H., Litscher, G., Watanabe, N., Wei, W., Hashimoto, T., Iwatsubo, T., et al. (2022). ALS-linked cytoplasmic FUS assemblies are compositionally different from physiological stress granules and sequester hnRNPA3, a novel modifier of FUS toxicity. Neurobiol. Dis. 162, 105585. doi:10.1016/j.nbd.2021.105585 | |

Banani, S. F., Lee, H. O., Hyman, A. A., and Rosen, M. K. (2017). Biomolecular condensates: Organizers of cellular biochemistry. Nat. Rev. Mol. Cell Biol. 18, 285–298. doi:10.1038/nrm.2017.7 | |

Baskerville, V., Rapuri, S., Mehlhop, E., & Coyne, A. N. (2023). SUN1 facilitates CHMP7 nuclear influx and injury cascades in sporadic amyotrophic lateral sclerosis. Brain : a journal of neurology, 147(1), 109–121. https://doi.org/10.1093/brain/awad291

Batra, R., Nelles, D. A., Pirie, E., Blue, S. M., Marina, R. J., Wang, H., et al. (2017). Elimination of toxic microsatellite repeat expansion RNA by RNA-targeting Cas9. Cell 170, 899–912. doi:10.1016/j.cell.2017.07.010 | |

Bauer, K. E., Bargenda, N., Schieweck, R., Illig, C., Segura, I., Harner, M., et al. (2022). RNA supply drives physiological granule assembly in neurons. Nat. Commun. 13, 2781. doi:10.1038/s41467-022-30067-3 | |

Baxi, E. G., Thompson, T., Li, J., Kaye, J. A., Lim, R. G., Wu, J., Ramamoorthy, D., Lima, L., Vaibhav, V., Matlock, A., Frank, A., Coyne, A. N., Landin, B., Ornelas, L., Mosmiller, E., Thrower, S., Farr, S. M., Panther, L., Gomez, E., Galvez, E., … Rothstein, J. D. (2022). Answer ALS, a large-scale resource for sporadic and familial ALS combining clinical and multi-omics data from induced pluripotent cell lines. Nature neuroscience, 25(2), 226–237. https://doi.org/10.1038/s41593-021-01006-0

Begovich, K., Vu, A. Q., Yeo, G., & Wilhelm, J. E. (2020). Conserved metabolite regulation of stress granule assembly via AdoMet. The Journal of cell biology, 219(8), e201904141.
Benhalevy, D., Anastasakis, D. G., and Hafner, M. (2018). Proximity-CLIP provides a snapshot of protein-occupied RNA elements in subcellular compartments. Nat. Methods 15, 1074–1082. doi:10.1038/s41592-018-0220-y | |

Bentmann, E., Neumann, M., Tahirovic, S., Rodde, R., Dormann, D., and Haass, C. (2012). Requirements for stress granule recruitment of fused in sarcoma (FUS) and TAR DNA-binding protein of 43 kDa (TDP-43). J. Biol. Chem. 287, 23079–23094. doi:10.1074/jbc.M111.328757 | |

Blauw, H. M., Barnes, C. P., van Vught, P. W., van Rheenen, W., Verheul, M., Cuppen, E., Veldink, J. H., & van den Berg, L. H. (2012). SMN1 gene duplications are associated with sporadic ALS. Neurology, 78(11), 776–780.

Blue, S. M., Yee, B. A., Pratt, G. A., Mueller, J. R., Park, S. S., Shishkin, A. A., et al. (2022). Transcriptome-wide identification of RNA-binding protein binding sites using seCLIP-seq. Nat. Protoc. 17, 1223–1265. doi:10.1038/s41596-022-00680-z | |

Boeynaems, S., Holehouse, A. S., Weinhardt, V., Kovacs, D., Van Lindt, J., Larabell, C., et al. (2019). Spontaneous driving forces give rise to protein-RNA condensates with coexisting phases and complex material properties. Proc. Natl. Acad. Sci. U. S. A. 116, 7889–7898. doi:10.1073/pnas.1821038116 | |

Bose, M., Lampe, M., Mahamid, J., and Ephrussi, A. (2022). Liquid-to-solid phase transition of oskar ribonucleoprotein granules is essential for their function in Drosophila embryonic development. Cell 185, 1308–1324.e23. doi:10.1016/j.cell.2022.02.022 | |

Bounedjah, O., Desforges, B., Wu, T. D., Pioche-Durieu, C., Marco, S., Hamon, L., et al. (2014). Free mRNA in excess upon polysome dissociation is a scaffold for protein multimerization to form stress granules. Nucleic Acids Res. 42, 8678–8691. doi:10.1093/nar/gku582 | |

Bowden, H. A., and Dormann, D. (2016). Altered mRNP granule dynamics in FTLD pathogenesis. J. Neurochem. 138 (1), 112–133. doi:10.1111/jnc.13601 | |

Boyle, E. A., Her, H. L., Mueller, J. R., Naritomi, J. T., Nguyen, G. G., & Yeo, G. W. (2023). Skipper analysis of eCLIP datasets enables sensitive detection of constrained translation factor binding sites. Cell genomics, 3(6), 100317.

Bruderer, R., Bernhardt, O. M., Gandhi, T., Miladinović, S. M., Cheng, L. Y., Messner, S., Ehrenberger, T., Zanotelli, V., Butscheid, Y., Escher, C., Vitek, O., Rinner, O., & Reiter, L. (2015). Extending the limits of quantitative proteome profiling with data-independent acquisition and application to acetaminophen-treated three-dimensional liver microtissues. Molecular & cellular proteomics : MCP, 14(5), 1400–1410.

Buchan, J. R., Muhlrad, D., and Parker, R. (2008). P bodies promote stress granule assembly in Saccharomyces cerevisiae. J. Cell Biol. 183, 441–455. doi:10.1083/jcb.200807043 | |
Buchan, J. R., and Parker, R. (2009). Eukaryotic stress granules: The ins and outs of translation. Mol. Cell 36, 932–941. doi:10.1016/j.molcel.2009.11.020 | |

Cao, Q., Boyer, D. R., Sawaya, M. R., Ge, P., and Eisenberg, D. S. (2019). Cryo-EM structures of four polymorphic TDP-43 amyloid cores. Nat. Struct. Mol. Biol. 26, 619–627. doi:10.1038/s41594-019-0248-4 | |

Cauchi R. J. (2014). Gem depletion: amyotrophic lateral sclerosis and spinal muscular atrophy crossover. CNS neuroscience & therapeutics, 20(7), 574–581.

Charizanis, K., Lee, K. Y., Batra, R., Goodwin, M., Zhang, C., Yuan, Y., et al. (2012). Muscleblind-like 2-mediated alternative splicing in the developing brain and dysregulation in myotonic dystrophy. Neuron 75, 437–450. doi:10.1016/j.neuron.2012.05.029 | |

Chew, J., Cook, C., Gendron, T. F., Jansen-West, K., Del Rosso, G., Daughrity, L. M., et al. (2019). Aberrant deposition of stress granule-resident proteins linked to C9orf72-associated TDP-43 proteinopathy. Mol. Neurodegener. 14, 9. doi:10.1186/s13024-019-0310-z | |

Choi, J. M., Hyman, A. A., and Pappu, R. V. (2020). Generalized models for bond percolation transitions of associative polymers. Phys. Rev. E 102, 042403. doi:10.1103/PhysRevE.102.042403 | |

Chou, C. C., Zhang, Y., Umoh, M. E., Vaughan, S. W., Lorenzini, I., Liu, F., Sayegh, M., Donlin-Asp, P. G., Chen, Y. H., Duong, D. M., Seyfried, N. T., Powers, M. A., Kukar, T., Hales, C. M., Gearing, M., Cairns, N. J., Boylan, K. B., Dickson, D. W., Rademakers, R., Zhang, Y. J., … Rossoll, W. (2018). TDP-43 pathology disrupts nuclear pore complexes and nucleocytoplasmic transport in ALS/FTD. Nature neuroscience, 21(2), 228–239.

Chu, Q., Wang, J., Du, Y., Zhou, T., Shi, A., Xiong, J., Ji, W. K., & Deng, L. (2023). Oligomeric CHMP7 mediates three-way ER junctions and ER-mitochondria interactions. Cell death and differentiation, 30(1), 94–110.

Corley, M., Flynn, R. A., Lee, B., Blue, S. M., Chang, H. Y., and Yeo, G. W. (2020). Footprinting SHAPE-eCLIP reveals transcriptome-wide hydrogen bonds at RNA-protein interfaces. Mol. Cell 80, 903–914. doi:10.1016/j.molcel.2020.11.014 | |

Coyne, A. N., Baskerville, V., Zaepfel, B. L., Dickson, D. W., Rigo, F., Bennett, F., Lusk, C. P., & Rothstein, J. D. (2021). Nuclear accumulation of CHMP7 initiates nuclear pore complex injury and subsequent TDP-43 dysfunction in sporadic and familial ALS. Science translational medicine, 13(604), eabe1923.

Coyne, A. N., Zaepfel, B. L., Hayes, L., Fitchman, B., Salzberg, Y., Luo, E. C., Bowen, K., Trost, H., Aigner, S., Rigo, F., Yeo, G. W., Harel, A., Svendsen, C. N., Sareen, D., & Rothstein, J. D. (2020). G4C2 Repeat RNA Initiates a POM121-Mediated Reduction in Specific Nucleoporins in C9orf72 ALS/FTD. Neuron, 107(6), 1124–1140.e11.

D'Angelo, M. A., Raices, M., Panowski, S. H., & Hetzer, M. W. (2009). Age-dependent deterioration of nuclear pore complexes causes a loss of nuclear integrity in postmitotic cells. Cell, 136(2), 284–295.

Daigle, J. G., Krishnamurthy, K., Ramesh, N., Casci, I., Monaghan, J., Mcavoy, K., et al. (2016). Pur-alpha regulates cytoplasmic stress granule dynamics and ameliorates FUS toxicity. Acta Neuropathol. 131, 605–620. doi:10.1007/s00401-015-1530-0 | |

Decker, C. J., Burke, J. M., Mulvaney, P. K., and Parker, R. (2022). RNA is required for the integrity of multiple nuclear and cytoplasmic membrane-less RNP granules. EMBO J. 41, e110137. doi:10.15252/embj.2021110137 | |

Dejesus-Hernandez, M., Mackenzie, I. R., Boeve, B. F., Boxer, A. L., Baker, M., Rutherford, N. J., et al. (2011). Expanded GGGGCC hexanucleotide repeat in noncoding region of C9ORF72

causes chromosome 9p-linked FTD and ALS. Neuron 72, 245–256. doi:10.1016/j.neuron.2011.09.011 | |

Dobin, A., Davis, C. A., Schlesinger, F., Drenkow, J., Zaleski, C., Jha, S., Batut, P., Chaisson, M., & Gingeras, T. R. (2013). STAR: ultrafast universal RNA-seq aligner. Bioinformatics (Oxford, England), 29(1), 15–21.

Eden, E., Navon, R., Steinfeld, I., Lipson, D., & Yakhini, Z. (2009). GOrilla: a tool for discovery and visualization of enriched GO terms in ranked gene lists. BMC bioinformatics, 10, 48.
Elbaum-Garfinkle, S., Kim, Y., Szczepaniak, K., Chen, C. C., Eckmann, C. R., Myong, S., et al. (2015). The disordered P granule protein LAF-1 drives phase separation into droplets with tunable viscosity and dynamics. Proc. Natl. Acad. Sci. U. S. A. 112, 7189–7194. doi:10.1073/pnas.1504822112 | |

Elmsaouri, S., Markmiller, S., and Yeo, G. W. (2022). APEX proximity labeling of stress granule proteins. Methods Mol. Biol. 2428, 381–399. doi:10.1007/978-1-0716-1975-9_23 | |

Fang, M. Y., Markmiller, S., Vu, A. Q., Javaherian, A., Dowdle, W. E., Jolivet, P., et al. (2019). Small-molecule modulation of TDP-43 recruitment to stress granules prevents persistent TDP-43 accumulation in ALS/FTD. Neuron 103, 802–819. doi:10.1016/j.neuron.2019.05.048 | |

Felisberto-Rodrigues, C., Thomas, J. C., McAndrew, C., Le Bihan, Y. V., Burke, R., Workman, P., & van Montfort, R. L. M. (2019). Structural and functional characterisation of human RNA helicase DHX8 provides insights into the mechanism of RNA-stimulated ADP release. The Biochemical journal, 476(18), 2521–2543.

Fonda, B. D., Jami, K. M., Boulos, N. R., and Murray, D. T. (2021). Identification of the rigid core for aged liquid droplets of an RNA-binding protein low complexity domain. J. Am. Chem. Soc. 143, 6657–6668. doi:10.1021/jacs.1c02424 | |

Fornerod, M., & Ohno, M. (2002). Exportin-mediated nuclear export of proteins and ribonucleoproteins. Results and problems in cell differentiation, 35, 67–91.

French, R. L., Grese, Z. R., Aligireddy, H., Dhavale, D. D., Reeb, A. N., Kedia, N., et al. (2019). Detection of TAR DNA-binding protein 43 (TDP-43) oligomers as initial intermediate species during aggregate formation. J. Biol. Chem. 294, 6696–6709. doi:10.1074/jbc.RA118.005889 | |

Fuller, G. G., Han, T., Freeberg, M. A., Moresco, J. J., Ghanbari Niaki, A., Roach, N. P., et al. (2020). RNA promotes phase separation of glycolysis enzymes into yeast G bodies in hypoxia. Elife 9, e48480. doi:10.7554/eLife.48480 |
|
Furukawa, Y., Kaneko, K., Matsumoto, G., Kurosawa, M., and Nukina, N. (2009). Cross-seeding fibrillation of Q/N-rich proteins offers new pathomechanism of polyglutamine diseases. J. Neurosci. 29, 5153–5162. doi:10.1523/JNEUROSCI.0783-09.2009 | |

Ganser, L. R., and Myong, S. (2020). Methods to study phase-separated condensates and the underlying molecular interactions. Trends biochem. Sci. 45, 1004–1005. doi:10.1016/j.tibs.2020.05.011 | |

Garcia-Jove Navarro, M., Kashida, S., Chouaib, R., Souquere, S., Pierron, G., Weil, D., et al. (2019). RNA is a critical element for the sizing and the composition of phase-separated RNA–protein condensates. Nat. Commun. 10, 3230. doi:10.1038/s41467-019-11241-6 | |

Gatta, A. T., Olmos, Y., Stoten, C. L., Chen, Q., Rosenthal, P. B., & Carlton, J. G. (2021). CDK1 controls CHMP7-dependent nuclear envelope reformation. eLife, 10, e59999.

Gertz, B., Wong, M., & Martin, L. J. (2012). Nuclear localization of human SOD1 and mutant SOD1-specific disruption of survival motor neuron protein complex in transgenic amyotrophic lateral sclerosis mice. Journal of neuropathology and experimental neurology, 71(2), 162–177.

Ghosh, S., and Geahlen, R. L. (2015). Stress granules modulate SYK to cause microglial cell dysfunction in alzheimer's disease. EBioMedicine 2, 1785–1798. doi:10.1016/j.ebiom.2015.09.053 | |

Gilks, N., Kedersha, N., Ayodele, M., Shen, L., Stoecklin, G., Dember, L. M., et al. (2004). Stress granule assembly is mediated by prion-like aggregation of TIA-1. Mol. Biol. Cell 15, 5383–5398. doi:10.1091/mbc.e04-08-0715 | |

Gleixner, A. M., Verdone, B. M., Otte, C. G., Anderson, E. N., Ramesh, N., Shapiro, O. R., et al. (2022). NUP62 localizes to ALS/FTLD pathological assemblies and contributes to TDP-43 insolubility. Nat. Commun. 13, 3380. doi:10.1038/s41467-022-31098-6 | |

Gonzalez, A., Mannen, T., Çağatay, T., Fujiwara, A., Matsumura, H., Niesman, A. B., et al. (2021). Mechanism of karyopherin-β2 binding and nuclear import of ALS variants FUS(P525L) and FUS(R495X). Sci. Rep. 11, 3754. doi:10.1038/s41598-021-83196-y | |

Gotz, J., Chen, F., Van Dorpe, J., and Nitsch, R. M. (2001). Formation of neurofibrillary tangles in P301l tau transgenic mice induced by Abeta 42 fibrils. Science 293, 1491–1495. doi:10.1126/science.1062097 | |

Grimm, C., Chari, A., Pelz, J. P., Kuper, J., Kisker, C., Diederichs, K., Stark, H., Schindelin, H., & Fischer, U. (2013). Structural basis of assembly chaperone- mediated snRNP formation. Molecular cell, 49(4), 692–703.

Groen, E. J., Fumoto, K., Blokhuis, A. M., Engelen-Lee, J., Zhou, Y., van den Heuvel, D. M., Koppers, M., van Diggelen, F., van Heest, J., Demmers, J. A., Kirby, J., Shaw, P. J., Aronica, E., Spliet, W. G., Veldink, J. H., van den Berg, L. H., & Pasterkamp, R. J. (2013). ALS-associated mutations in FUS disrupt the axonal distribution and function of SMN. Human molecular genetics, 22(18), 3690–3704.

Gu, M., LaJoie, D., Chen, O. S., von Appen, A., Ladinsky, M. S., Redd, M. J., Nikolova, L., Bjorkman, P. J., Sundquist, W. I., Ullman, K. S., & Frost, A. (2017). LEM2 recruits CHMP7 for ESCRT-mediated nuclear envelope closure in fission yeast and human cells. Proceedings of the National Academy of Sciences of the United States of America, 114(11), E2166–E2175.

Guillen-Boixet, J., Kopach, A., Holehouse, A. S., Wittmann, S., Jahnel, M., Schlussler, R., et al. (2020). RNA-induced conformational switching and clustering of G3BP drive stress granule assembly by condensation. Cell 181, 346–361. doi:10.1016/j.cell.2020.03.049 | |

Guise, A. J., Misal, S. A., Carson, R., Boekweg, H., Van Der Watt, D., Truong, T., Liang, Y., Chu, J. H., Welsh, N. C., Gagnon, J., Payne, S. H., Plowey, E. D., & Kelly, R. T. (2023). TDP-43-stratified single-cell proteomic profiling of postmortem human spinal motor neurons reveals protein dynamics in amyotrophic lateral sclerosis. bioRxiv : the preprint server for biology, 2023.06.08.544233.

Guo, L., Kim, H. J., Wang, H., Monaghan, J., Freyermuth, F., Sung, J. C., et al. (2018). Nuclear-import receptors reverse aberrant phase transitions of RNA-binding proteins with prion-like domains. Cell 173, 677–692. doi:10.1016/j.cell.2018.03.002 | |

Gwon, Y., Maxwell, B. A., Kolaitis, R. M., Zhang, P., Kim, H. J., and Taylor, J. P. (2021). Ubiquitination of G3BP1 mediates stress granule disassembly in a context-specific manner. Science 372, eabf6548. doi:10.1126/science.abf6548 | |

Hallegger, M., Chakrabarti, A. M., Lee, F. C. Y., Lee, B. L., Amalietti, A. G., Odeh, H. M., et al. (2021). TDP-43 condensation properties specify its RNA-binding and regulatory repertoire. Cell 184, 4680–4696.e22. doi:10.1016/j.cell.2021.07.018 | |

Harada, Y., Sutomo, R., Sadewa, A. H., Akutsu, T., Takeshima, Y., Wada, H., Matsuo, M., & Nishio, H. (2002). Correlation between SMN2 copy number and clinical phenotype of spinal muscular atrophy: three SMN2 copies fail to rescue some patients from the disease severity. Journal of neurology, 249(9), 1211–1219.

Harding, H. P., Novoa, I., Zhang, Y., Zeng, H., Wek, R., Schapira, M., et al. (2000). Regulated translation initiation controls stress-induced gene expression in mammalian cells. Mol. Cell 6, 1099–1108. doi:10.1016/s1097-2765(00)00108-8 | |

Harmon, T. S., Holehouse, A. S., Rosen, M. K., and Pappu, R. V. (2017). Intrinsically disordered linkers determine the interplay between phase separation and gelation in multivalent proteins. Elife 6, e30294. doi:10.7554/eLife.30294 | |

Hayes, L. R., Duan, L., Bowen, K., Kalab, P., & Rothstein, J. D. (2020). C9orf72 arginine-rich dipeptide repeat proteins disrupt karyopherin-mediated nuclear import. eLife, 9, e51685.

Her, H. L., Boyle, E., & Yeo, G. W. (2022). Metadensity: a background-aware python pipeline for summarizing CLIP signals on various transcriptomic sites. Bioinformatics advances, 2(1), vbac083. https://doi.org/10.1093/bioadv/vbac083

Hofweber, M., Hutten, S., Bourgeois, B., Spreitzer, E., Niedner-Boblenz, A., Schifferer, M., et al. (2018). Phase separation of FUS is suppressed by its nuclear import receptor and arginine methylation. Cell 173, 706–719. doi:10.1016/j.cell.2018.03.004 | |

Hondele, M., Sachdev, R., Heinrich, S., Wang, J., Vallotton, P., Fontoura, B. M. A., et al. (2019). DEAD-box ATPases are global regulators of phase-separated organelles. Nature 573, 144–148. doi:10.1038/s41586-019-1502-y | |

Horvathova, I., Voigt, F., Kotrys, A. V., Zhan, Y., Artus-Revel, C. G., Eglinger, J., et al. (2017). The dynamics of mRNA turnover revealed by single-molecule imaging in single cells. Mol. Cell 68, 615–625. doi:10.1016/j.molcel.2017.09.030 | |

Hutten, S., and Dormann, D. (2020). Nucleocytoplasmic transport defects in neurodegeneration - cause or consequence? Semin. Cell Dev. Biol. 99, 151–162. doi:10.1016/j.semcdb.2019.05.020 | |

Irgen-Gioro, S., Walling, V., and Chong, S. (2022). Fixation can change the appearance of phase separation in living cells, bioRxiv 2005. 490956.

Iserman, C., Desroches Altamirano, C., Jegers, C., Friedrich, U., Zarin, T., Fritsch, A. W., et al. (2020). Condensation of Ded1p promotes a translational switch from housekeeping to stress protein production. Cell 181, 818–831. doi:10.1016/j.cell.2020.04.009 | |

Ivanov, P., Kedersha, N., and Anderson, P. (2011). Stress puts TIA on TOP. Genes Dev. 25, 2119–2124. doi:10.1101/gad.17838411 | |

Jain, A., and Vale, R. D. (2017). RNA phase transitions in repeat expansion disorders. Nature 546, 243–247. doi:10.1038/nature22386 | |

Jawerth, L., Fischer-Friedrich, E., Saha, S., Wang, J., Franzmann, T., Zhang, X., et al. (2020). Protein condensates as aging Maxwell fluids. Science 370, 1317–1323. doi:10.1126/science.aaw4951 | |

Jin, W., Brannan, K. W., Kapeli, K., Park, S. S., Tan, H. Q., Gosztyla, M. L., Mujumdar, M., Ahdout, J., Henroid, B., Rothamel, K., Xiang, J. S., Wong, L., & Yeo, G. W. (2023). HydRA: Deep-learning models for predicting RNA-binding capacity from protein interaction association context and protein sequence. Molecular cell, 83(14), 2595–2611.e11.

Jin, M., Fuller, G. G., Han, T., Yao, Y., Alessi, A. F., Freeberg, M. A., et al. (2017). Glycolytic enzymes coalesce in G bodies under hypoxic stress. Cell Rep. 20, 895–908. doi:10.1016/j.celrep.2017.06.082 | |

Jo, M., Lee, S., Jeon, Y. M., Kim, S., Kwon, Y., & Kim, H. J. (2020). The role of TDP-43 propagation in neurodegenerative diseases: integrating insights from clinical and experimental studies. Experimental & molecular medicine, 52(10), 1652–1662.

Kato, M., Han, T. W., Xie, S., Shi, K., Du, X., Wu, L. C., et al. (2012). Cell-free formation of RNA granules: Low complexity sequence domains form dynamic fibers within hydrogels. Cell 149, 753–767. doi:10.1016/j.cell.2012.04.017 | |

Khong, A., Matheny, T., Jain, S., Mitchell, S. F., Wheeler, J. R., and Parker, R. (2017). The stress granule transcriptome reveals principles of mRNA accumulation in stress granules. Mol. Cell 68, 808–820. e805. doi:10.1016/j.molcel.2017.10.015 | |

Kim, D. I., Jensen, S. C., Noble, K. A., Kc, B., Roux, K. H., Motamedchaboki, K., et al. (2016). An improved smaller biotin ligase for BioID proximity labeling. Mol. Biol. Cell 27, 1188–1196. doi:10.1091/mbc.E15-12-0844 | |

Kim, H. J., Kim, N. C., Wang, Y.-D., Scarborough, E. A., Moore, J., Diaz, Z., et al. (2013). Mutations in prion-like domains in hnRNPA2B1 and hnRNPA1 cause multisystem proteinopathy and ALS. Nature 495, 467–473. doi:10.1038/nature11922 | |

Klim, J. R., Williams, L. A., Limone, F., Guerra San Juan, I., Davis-Dusenbery, B. N., Mordes, D. A., Burberry, A., Steinbaugh, M. J., Gamage, K. K., Kirchner, R., Moccia, R., Cassel, S. H., Chen, K., Wainger, B. J., Woolf, C. J., & Eggan, K. (2019). ALS-implicated protein TDP-43 sustains levels of STMN2, a mediator of motor neuron growth and repair. Nature neuroscience, 22(2), 167–179.

Krach, F., Wheeler, E. C., Regensburger, M., Boerstler, T., Wend, H., Vu, A. Q., Wang, R., Reischl, S., Boldt, K., Batra, R., Aigner, S., Ravits, J., Winkler, J., Yeo, G. W., & Winner, B. (2022). Aberrant NOVA1 function disrupts alternative splicing in early stages of amyotrophic lateral sclerosis. Acta neuropathologica, 144(3), 413–435. https://doi.org/10.1007/s00401-022-02450-3

Krus, K. L., Strickland, A., Yamada, Y., Devault, L., Schmidt, R. E., Bloom, A. J., Milbrandt, J., & DiAntonio, A. (2022). Loss of Stathmin-2, a hallmrk of TDP-43-associated ALS, causes motor neuropathy. Cell reports, 39(13), 111001.

Labbadia, J., and Morimoto, R. I. (2013). Huntington's disease: Underlying molecular mechanisms and emerging concepts. Trends biochem. Sci. 38, 378–385. doi:10.1016/j.tibs.2013.05.003 | |

Laghmach, R., Alshareedah, I., Pham, M., Raju, M., Banerjee, P. R., and Potoyan, D. A. (2022). RNA chain length and stoichiometry govern surface tension and stability of protein-RNA condensates. iScience 25, 104105. doi:10.1016/j.isci.2022.104105 | |

Le, P., Ahmed, N., and Yeo, G. W. (2022). Illuminating RNA biology through imaging. Nat. Cell Biol. 24, 815–824. doi:10.1038/s41556-022-00933-9 | |

Lee, C. S., Putnam, A., Lu, T., He, S., Ouyang, J. P. T., and Seydoux, G. (2020). Recruitment of mRNAs to P granules by condensation with intrinsically-disordered proteins. Elife 9, e52896. doi:10.7554/eLife.52896 | |

Lee, J. E., Bennett, C. F., and Cooper, T. A. (2012). RNase H-mediated degradation of toxic RNA in myotonic dystrophy type 1. Proc. Natl. Acad. Sci. U. S. A. 109, 4221–4226. doi:10.1073/pnas.1117019109 | |

Lehmkuhl, E. M., & Zarnescu, D. C. (2018). Lost in Translation: Evidence for Protein Synthesis Deficits in ALS/FTD and Related Neurodegenerative Diseases. Advances in neurobiology, 20, 283–301.

Li, L., Liu, H., Dong, P., Li, D., Legant, W. R., Grimm, J. B., et al. (2016). Real-time imaging of Huntingtin aggregates diverting target search and gene transcription. Elife 5, e17056. doi:10.7554/eLife.17056 | |

Li, W., Xu, H., Xiao, T., Cong, L., Love, M. I., Zhang, F., Irizarry, R. A., Liu, J. S., Brown, M., & Liu, X. S. (2014). MAGeCK enables robust identification of essential genes from genome-scale CRISPR/Cas9 knockout screens. Genome biology, 15(12), 554.

Liao, Y., Smyth, G. K., & Shi, W. (2014). featureCounts: an efficient general purpose program for assigning sequence reads to genomic features. Bioinformatics (Oxford, England), 30(7), 923–930.

Lim, J., and Yue, Z. (2015). Neuronal aggregates: Formation, clearance, and spreading. Dev. Cell 32, 491–501. doi:10.1016/j.devcel.2015.02.002 | |

Linsenmeier, M., Hondele, M., Grigolato, F., Secchi, E., Weis, K., and Arosio, P. (2022). Dynamic arrest and aging of biomolecular condensates are modulated by low-complexity domains, RNA and biochemical activity. Nat. Commun. 13, 3030. doi:10.1038/s41467-022-30521-2 | |

Liu, Q., Fischer, U., Wang, F., & Dreyfuss, G. (1997). The spinal muscular atrophy disease gene product, SMN, and its associated protein SIP1 are in a complex with spliceosomal snRNP proteins. Cell, 90(6), 1013–1021.

Liu, Q., & Dreyfuss, G. (1996). A novel nuclear structure containing the survival of motor neurons protein. The EMBO journal, 15(14), 3555–3565.

Liu, Y., Iqbal, A., Li, W., Ni, Z., Wang, Y., Ramprasad, J., Abraham, K. J., Zhang, M., Zhao, D. Y., Qin, S., Loppnau, P., Jiang, H., Guo, X., Brown, P. J., Zhen, X., Xu, G., Mekhail, K., Ji, X., Bedford, M. T., Greenblatt, J. F., … Min, J. (2022). A small molecule antagonist of SMN disrupts the interaction between SMN and RNAP II. Nature communications, 13(1), 5453.

Liu-Yesucevitz, L., Bilgutay, A., Zhang, Y. J., Vanderweyde, T., Citro, A., Mehta, T., et al. (2010). Tar DNA binding protein-43 (TDP-43) associates with stress granules: Analysis of cultured cells and pathological brain tissue. PLoS One 5, e13250. doi:10.1371/journal.pone.0013250 | |

Love, M. I., Huber, W., & Anders, S. (2014). Moderated estimation of fold change and dispersion for RNA-seq data with DESeq2. Genome biology, 15(12), 550.

Lu, S., Hu, J., Aladesuyi, B., Goginashvili, A., Vazquez-Sanchez, S., Diedrich, J., et al. (2021). Heat shock chaperone HSPB1 regulates cytoplasmic TDP-43 phase separation and liquid-to-gel transition. bioRxiv 2010, 464447.

Ma, Y., Li, H., Gong, Z., Yang, S., Wang, P., and Tang, C. (2022). Nucleobase clustering contributes to the formation and hollowing of repeat-expansion RNA condensate. J. Am. Chem. Soc. 144, 4716–4720. doi:10.1021/jacs.1c12085 | |

Maharana, S., Wang, J., Papadopoulos, D. K., Richter, D., Pozniakovsky, A., Poser, I., et al. (2018). RNA buffers the phase separation behavior of prion-like RNA binding proteins. Science 360, 918–921. doi:10.1126/science.aar7366 | |

Majerciak, V., Zhou, T., and Zheng, Z.-M. (2021). RNA helicase DDX6 in P-bodies is essential for the assembly of stress granules. bioRxiv 2009, 461736.

Makarov, E. M., Owen, N., Bottrill, A., & Makarova, O. V. (2012). Functional mammalian spliceosomal complex E contains SMN complex proteins in addition to U1 and U2 snRNPs. Nucleic acids research, 40(6), 2639–2652.

Mandelboim, M., Barth, S., Biton, M., Liang, X. H., & Michaeli, S. (2003). Silencing of Sm proteins in Trypanosoma brucei by RNA interference captured a novel cytoplasmic intermediate in spliced leader RNA biogenesis. The Journal of biological chemistry, 278(51), 51469–51478.

Mann, J. R., Gleixner, A. M., Mauna, J. C., Gomes, E., Dechellis-Marks, M. R., Needham, P. G., et al. (2019). RNA binding antagonizes neurotoxic phase transitions of TDP-43. Neuron 102, 321–338. doi:10.1016/j.neuron.2019.01.048 | |

Markmiller, S., Soltanieh, S., Server, K. L., Mak, R., Jin, W., Fang, M. Y., et al. (2018). Context-dependent and disease-specific diversity in protein interactions within stress granules. Cell 172, 590–604. doi:10.1016/j.cell.2017.12.032 | |

Markmiller, S., Sathe, S., Server, K. L., Nguyen, T. B., Fulzele, A., Cody, N., et al. (2021). Persistent mRNA localization defects and cell death in ALS neurons caused by transient cellular stress. Cell Rep. 36, 109685. doi:10.1016/j.celrep.2021.109685 | |

Markmiller, S., Soltanieh, S., Server, K. L., Mak, R., Jin, W., Fang, M. Y., Luo, E. C., Krach, F., Yang, D., Sen, A., Fulzele, A., Wozniak, J. M., Gonzalez, D. J., Kankel, M. W., Gao, F. B., Bennett, E. J., Lécuyer, E., & Yeo, G. W. (2018). Context-Dependent and Disease-Specific Diversity in Protein Interactions within Stress Granules. Cell, 172(3), 590–604.e13.

Marmor-Kollet, H., Siany, A., Kedersha, N., Knafo, N., Rivkin, N., Danino, Y. M., et al. (2020). Spatiotemporal proteomic analysis of stress granule disassembly using APEX reveals regulation

by SUMOylation and links to ALS pathogenesis. Mol. Cell 80, 876–891. doi:10.1016/j.molcel.2020.10.032 | |

Massenet, S., Pellizzoni, L., Paushkin, S., Mattaj, I. W., & Dreyfuss, G. (2002). The SMN complex is associated with snRNPs throughout their cytoplasmic assembly pathway. Molecular and cellular biology, 22(18), 6533–6541.

Mateju, D., Eichenberger, B., Voigt, F., Eglinger, J., Roth, G., and Chao, J. A. (2020). Single-molecule imaging reveals translation of mRNAs localized to stress granules. Cell 183, 1801–1812. doi:10.1016/j.cell.2020.11.010 | |

Mateju, D., Franzmann, T. M., Patel, A., Kopach, A., Boczek, E. E., Maharana, S., et al. (2017). An aberrant phase transition of stress granules triggered by misfolded protein and prevented by chaperone function. EMBO J. 36, 1669–1687. doi:10.15252/embj.201695957 | |

Matheny, T., Rao, B. S., and Parker, R. (2019). Transcriptome-Wide comparison of stress granules and P-bodies reveals that translation plays a major role in RNA partitioning. Mol. Cell. Biol. 39, e00313-19. doi:10.1128/MCB.00313-19 | |

Mathieu, C., Pappu, R. V., and Taylor, J. P. (2020). Beyond aggregation: Pathological phase transitions in neurodegenerative disease. Science 370, 56–60. doi:10.1126/science.abb8032 | |
Matos, C. A., De Almeida, L. P., and Nobrega, C. (2019). Machado-joseph disease/spinocerebellar ataxia type 3: Lessons from disease pathogenesis and clues into therapy. J. Neurochem. 148, 8–28. doi:10.1111/jnc.14541 | |

Maxwell, B. A., Gwon, Y., Mishra, A., Peng, J., Nakamura, H., Zhang, K., et al. (2021). Ubiquitination is essential for recovery of cellular activities after heat shock. Science 372, eabc3593. doi:10.1126/science.abc3593 | |

Meister, G., Hannus, S., Plöttner, O., Baars, T., Hartmann, E., Fakan, S., Laggerbauer, B., & Fischer, U. (2001). SMNrp is an essential pre-mRNA splicing factor required for the formation of the mature spliceosome. The EMBO journal, 20(9), 2304–2314.

Melamed, Z., López-Erauskin, J., Baughn, M. W., Zhang, O., Drenner, K., Sun, Y., Freyermuth, F., McMahon, M. A., Beccari, M. S., Artates, J. W., Ohkubo, T., Rodriguez, M., Lin, N., Wu, D., Bennett, C. F., Rigo, F., Da Cruz, S., Ravits, J., Lagier-Tourenne, C., & Cleveland, D. W. (2019). Premature polyadenylation-mediated loss of stathmin-2 is a hallmark of TDP-43-dependent neurodegeneration. Nature neuroscience, 22(2), 180–190.

Mittag, T., and Pappu, R. V. (2022). A conceptual framework for understanding phase separation and addressing open questions and challenges. Mol. Cell 82, 2201–2214. doi:10.1016/j.molcel.2022.05.018 | |

Molliex, A., Temirov, J., Lee, J., Coughlin, M., Kanagaraj, A. P., Kim, H. J., et al. (2015). Phase separation by low complexity domains promotes stress granule assembly and drives pathological fibrillization. Cell 163, 123–133. doi:10.1016/j.cell.2015.09.015 | |

Moon, S. L., Morisaki, T., Stasevich, T. J., and Parker, R. (2020). Coupling of translation quality control and mRNA targeting to stress granules. J. Cell Biol. 219, e202004120. doi:10.1083/jcb.202004120 | |

Murray, D. T., Kato, M., Lin, Y., Thurber, K. R., Hung, I., Mcknight, S. L., et al. (2017). Structure of FUS protein fibrils and its relevance to self-assembly and phase separation of low-complexity domains. Cell 171, 615–627. doi:10.1016/j.cell.2017.08.048 | |

Niaki, A. G., Sarkar, J., Cai, X., Rhine, K., Vidaurre, V., Guy, B., et al. (2020). Loss of dynamic RNA interaction and aberrant phase separation induced by two distinct types of ALS/FTD-Linked FUS mutations. Mol. Cell 77, 82–94. doi:10.1016/j.molcel.2019.09.022 | |

Niranjanakumari, S., Lasda, E., Brazas, R., and Garcia-Blanco, M. A. (2002). Reversible cross-linking combined with immunoprecipitation to study RNA-protein interactions in vivo. Methods 26, 182–190. doi:10.1016/S1046-2023(02)00021-X | |

Nomura, T., Watanabe, S., Kaneko, K., Yamanaka, K., Nukina, N., and Furukawa, Y. (2014). Intranuclear aggregation of mutant FUS/TLS as a molecular pathomechanism of amyotrophic lateral sclerosis. J. Biol. Chem. 289, 1192–1202. doi:10.1074/jbc.M113.516492 | |

Odeh, H. M., Fare, C. M., and Shorter, J. (2022). Nuclear-import receptors counter deleterious phase transitions in neurodegenerative disease. J. Mol. Biol. 434, 167220. doi:10.1016/j.jmb.2021.167220 | |

Olmos, Y., Perdrix-Rosell, A., & Carlton, J. G. (2016). Membrane Binding by CHMP7 Coordinates ESCRT-III-Dependent Nuclear Envelope Reformation. Current biology : CB, 26(19), 2635–2641.

Padron, A., Iwasaki, S., and Ingolia, N. T. (2019). Proximity RNA labeling by APEX-seq reveals the organization of translation initiation complexes and repressive RNA granules. Mol. Cell 75, 875–887. doi:10.1016/j.molcel.2019.07.030 | |

Patel, A., Lee, H. O., Jawerth, L., Maharana, S., Jahnel, M., Hein, M. Y., et al. (2015). A liquid-to-solid phase transition of the ALS protein FUS accelerated by disease mutation. Cell 162, 1066–1077. doi:10.1016/j.cell.2015.07.047 | |

Patel, A. A., & Steitz, J. A. (2003). Splicing double: insights from the second spliceosome. Nature reviews. Molecular cell biology, 4(12), 960–970.

Piao, Y., Hashimoto, T., Takahama, S., Kakita, A., Komori, T., Morita, T., Takahashi, H., Mizutani, T., & Oyanagi, K. (2011). Survival motor neuron (SMN) protein in the spinal anterior horn cells of patients with sporadic amyotrophic lateral sclerosis. Brain research, 1372, 152–159.

Pillai, R. S., Grimmler, M., Meister, G., Will, C. L., Lührmann, R., Fischer, U., & Schümperli, D. (2003). Unique Sm core structure of U7 snRNPs: assembly by a specialized SMN complex

and the role of a new component, Lsm11, in histone RNA processing. Genes & development, 17(18), 2321–2333.

Pushpalatha, K. V., Solyga, M., Nakamura, A., and Besse, F. (2022). RNP components condense into repressive RNP granules in the aging brain. Nat. Commun. 13, 2782. doi:10.1038/s41467-022-30066-4 | |

Raices, M., & D'Angelo, M. A. (2022). Analysis of Nuclear Pore Complex Permeability in Mammalian Cells and Isolated Nuclei Using Fluorescent Dextrans. Methods in molecular biology (Clifton, N.J.), 2502, 69–80.

Rappsilber, J., Mann, M., & Ishihama, Y. (2007). Protocol for micro-purification, enrichment, pre-fractionation and storage of peptides for proteomics using StageTips. Nature protocols, 2(8), 1896–1906.

Ray, S., Singh, N., Kumar, R., Patel, K., Pandey, S., Datta, D., et al. (2020). α-Synuclein aggregation nucleates through liquid–liquid phase separation. Nat. Chem. 12, 705–716. doi:10.1038/s41557-020-0465-9 | |

Reber, S., Jutzi, D., Lindsay, H., Devoy, A., Mechtersheimer, J., Levone, B. R., et al. (2021). The phase separation-dependent FUS interactome reveals nuclear and cytoplasmic function of liquid-liquid phase separation. Nucleic Acids Res. 49, 7713–7731. doi:10.1093/nar/gkab582 | | Reineke, L. C., and Neilson, J. R. (2019). Differences between acute and chronic stress granules, and how these differences may impact function in human disease. Biochem. Pharmacol. 162, 123–131. doi:10.1016/j.bcp.2018.10.009 | |

Rhine, K., Skanchy, S., and Myong, S. (2022b). Single-molecule and ensemble methods to probe RNP nucleation and condensate properties. Methods 197, 74–81. doi:10.1016/j.ymeth.2021.02.012 | |

Rhine, K., Vidaurre, V., and Myong, S. (2020b). RNA droplets. Annu. Rev. Biophys. 49, 247–265. doi:10.1146/annurev-biophys-052118-115508 | |

Rhine, K., Makurath, M. A., Liu, J., Skanchy, S., Lopez, C., Catalan, K. F., et al. (2020a). ALS/FTLD-Linked mutations in FUS Glycine residues cause accelerated gelation and reduced interactions with wild-type FUS. Mol. Cell 80, 666–681. doi:10.1016/j.molcel.2020.10.014 | | Rhine, K., Dasovich, M., Yoniles, J., Badiee, M., Skanchy, S., Ganser, L. R., et al. (2022a). Poly(ADP-ribose) drives condensation of FUS via a transient interaction. Mol. Cell 82, 969–985.e11. e911. doi:10.1016/j.molcel.2022.01.018 | |

Roberson, E. D., Scearce-Levie, K., Palop, J. J., Yan, F., Cheng, I. H., Wu, T., et al. (2007). Reducing endogenous tau ameliorates amyloid beta-induced deficits in an Alzheimer's disease mouse model. Science 316, 750–754. doi:10.1126/science.1141736 | |

Roden, C., and Gladfelter, A. S. (2021). RNA contributions to the form and function of biomolecular condensates. Nat. Rev. Mol. Cell Biol. 22, 183–195. doi:10.1038/s41580-020-0264-6 | |

Rodriguez-Muela, N., Litterman, N. K., Norabuena, E. M., Mull, J. L., Galazo, M. J., Sun, C., Ng, S. Y., Makhortova, N. R., White, A., Lynes, M. M., Chung, W. K., Davidow, L. S., Macklis, J. D., & Rubin, L. L. (2017). Single-Cell Analysis of SMN Reveals Its Broader Role in Neuromuscular Disease. Cell reports, 18(6), 1484–1498.

Rothstein, J. D., Warlick, C., & Coyne, A. N. (2023). Highly variable molecular signatures of TDP-43 loss of function are associated with nuclear pore complex injury in a population study of sporadic ALS patient iPSNs. bioRxiv : the preprint server for biology, 2023.12.12.571299. https://doi.org/10.1101/2023.12.12.571299

Rothstein, J. D., Baskerville, V., Rapuri, S., Mehlhop, E., Jafar-Nejad, P., Rigo, F., Bennett, F., Mizielinska, S., Isaacs, A., & Coyne, A. N. (2023). G2C4 targeting antisense oligonucleotides potently mitigate TDP-43 dysfunction in human C9orf72 ALS/FTD induced pluripotent stem cell derived neurons. Acta neuropathologica, 147(1), 1. https://doi.org/10.1007/s00401-023-02652-3

Roux, K. J., Kim, D. I., Raida, M., and Burke, B. (2012). A promiscuous biotin ligase fusion protein identifies proximal and interacting proteins in mammalian cells. J. Cell Biol. 196, 801–810. doi:10.1083/jcb.201112098 | |

Ryu, H. H., Jun, M. H., Min, K. J., Jang, D. J., Lee, Y. S., Kim, H. K., et al. (2014). Autophagy regulates amyotrophic lateral sclerosis-linked fused in sarcoma-positive stress granules in neurons. Neurobiol. Aging 35, 2822–2831. doi:10.1016/j.neurobiolaging.2014.07.026 | |

Sanchez-Burgos, I., Espinosa, J. R., Joseph, J. A., and Collepardo-Guevara, R. (2022). RNA length has a non-trivial effect in the stability of biomolecular condensates formed by RNA-binding proteins. PLoS Comput. Biol. 18, e1009810. doi:10.1371/journal.pcbi.1009810 | |

Schwartz, J. C., Wang, X., Podell, E. R., and Cech, T. R. (2013). RNA seeds higher-order assembly of FUS protein. Cell Rep. 5, 918–925. doi:10.1016/j.celrep.2013.11.017 | |

Shan, X., Chiang, P. M., Price, D. L., & Wong, P. C. (2010). Altered distributions of Gemini of coiled bodies and mitochondria in motor neurons of TDP-43 transgenic mice. Proceedings of the National Academy of Sciences of the United States of America, 107(37), 16325–16330.

Shen, H., Yanas, A., Owens, M. C., Zhang, C., Fritsch, C., Fare, C. M., et al. (2022a). Sexually dimorphic RNA helicases DDX3X and DDX3Y differentially regulate RNA metabolism through phase separation. Mol. Cell 82, 2588–2603.e9. doi:10.1016/j.molcel.2022.04.022 | |

Shen, Y., Chen, A., Wang, W., Shen, Y., Ruggeri, F. S., Aime, S., et al. (2022b). Solid/liquid coexistence during aging of FUS condensates. bioRxiv 2008, 503964. doi:10.1101/2022.08.15.503964 |

Shukla, S., & Parker, R. (2016). Hypo- and Hyper-Assembly Diseases of RNA-Protein Complexes. Trends in molecular medicine, 22(7), 615–628.

Sleigh, J. N., Tosolini, A. P., Gordon, D., Devoy, A., Fratta, P., Fisher, E. M. C., et al. (2020). Mice carrying ALS mutant TDP-43, but not mutant FUS, display in vivo defects in axonal transport of signaling endosomes. Cell Rep. 30, 3655–3662. doi:10.1016/j.celrep.2020.02.078 | |

Sreedharan, J., Blair, I. P., Tripathi, V. B., Hu, X., Vance, C., Rogelj, B., et al. (2008). TDP-43 mutations in familial and sporadic amyotrophic lateral sclerosis. Science 319, 1668–1672. doi:10.1126/science.1154584 | |

Stoten, C. L., & Carlton, J. G. (2018). ESCRT-dependent control of membrane remodelling during cell division. Seminars in cell & developmental biology, 74, 50–65. https://doi.org/10.1016/j.semcdb.2017.08.035

Tang, X., Bharath, S. R., Piao, S., Tan, V. Q., Bowler, M. W., & Song, H. (2016). Structural basis for specific recognition of pre-snRNA by Gemin5. Cell research, 26(12), 1353–1356.
Taylor, J. P., Brown, R. H., Jr, & Cleveland, D. W. (2016). Decoding ALS: from genes to mechanism. Nature, 539(7628), 197–206.

Thaller, D. J., Allegretti, M., Borah, S., Ronchi, P., Beck, M., & Lusk, C. P. (2019). An ESCRT-LEM protein surveillance system is poised to directly monitor the nuclear envelope and nuclear transport system. eLife, 8, e45284.

Thedieck, K., Holzwarth, B., Prentzell, M. T., Boehlke, C., Klasener, K., Ruf, S., et al. (2013). Inhibition of mTORC1 by astrin and stress granules prevents apoptosis in cancer cells. Cell 154, 859–874. doi:10.1016/j.cell.2013.07.031 | |

Tourriere, H., Chebli, K., Zekri, L., Courselaud, B., Blanchard, J. M., Bertrand, E., et al. (2003). The RasGAP-associated endoribonuclease G3BP assembles stress granules. J. Cell Biol. 160, 823–831. doi:10.1083/jcb.200212128 | |

Trcek, T., Douglas, T. E., Grosch, M., Yin, Y., Eagle, W. V. I., Gavis, E. R., et al. (2020). Sequence-independent self-assembly of germ granule mRNAs into homotypic clusters. Mol. Cell 78, 941–950. doi:10.1016/j.molcel.2020.05.008 | |
Tsuiji, H., Iguchi, Y., Furuya, A., Kataoka, A., Hatsuta, H., Atsuta, N., Tanaka, F., Hashizume, Y., Akatsu, H., Murayama, S., Sobue, G., & Yamanaka, K. (2013). Spliceosome integrity is defective in the motor neuron diseases ALS and SMA. EMBO molecular medicine, 5(2), 221–234.

Turner, B. J., Parkinson, N. J., Davies, K. E., & Talbot, K. (2009). Survival motor neuron deficiency enhances progression in an amyotrophic lateral sclerosis mouse model. Neurobiology of disease, 34(3), 511–517.

Uchihara, T., Fujigasaki, H., Koyano, S., Nakamura, A., Yagishita, S., and Iwabuchi, K. (2001). Non-expanded polyglutamine proteins in intranuclear inclusions of hereditary ataxias – triple-labeling immunofluorescence study. Acta Neuropathol. 102, 149–152. doi:10.1007/s004010100364 | |

Van Nostrand, E.L., Freese, P., Pratt, G.A. et al. A large-scale binding and functional map of human RNA-binding proteins. Nature 583, 711–719 (2020).

Van Nostrand, E. L., Pratt, G. A., Shishkin, A. A., Gelboin-Burkhart, C., Fang, M. Y., Sundararaman, B., et al. (2016). Robust transcriptome-wide discovery of RNA-binding protein binding sites with enhanced CLIP (eCLIP). Nat. Methods 13, 508–514. doi:10.1038/nmeth.3810

Van Nostrand, E. L., Pratt, G. A., Shishkin, A. A., Gelboin-Burkhart, C., Fang, M. Y., Sundararaman, B., Blue, S. M., Nguyen, T. B., Surka, C., Elkins, K., Stanton, R., Rigo, F., Guttman, M., & Yeo, G. W. (2016). Robust transcriptome-wide discovery of RNA-binding protein binding sites with enhanced CLIP (eCLIP). Nature methods, 13(6), 508–514.

Van Nostrand, E. L., Nguyen, T. B., Gelboin-Burkhart, C., Wang, R., Blue, S. M., Pratt, G. A., Louie, A. L., & Yeo, G. W. (2017). Robust, Cost-Effective Profiling of RNA Binding Protein Targets with Single-end Enhanced Crosslinking and Immunoprecipitation (seCLIP). Methods in molecular biology (Clifton, N.J.), 1648, 177–200.

Van Treeck, B., Protter, D. S. W., Matheny, T., Khong, A., Link, C. D., and Parker, R. (2018). RNA self-assembly contributes to stress granule formation and defining the stress granule transcriptome. Proc. Natl. Acad. Sci. U. S. A. 115, 2734–2739. doi:10.1073/pnas.1800038115 | |

Vance, C., Rogelj, B., Hortobagyi, T., De Vos, K. J., Nishimura, A. L., Sreedharan, J., et al. (2009). Mutations in FUS, an RNA processing protein, cause familial amyotrophic lateral sclerosis type 6. Science 323, 1208–1211. doi:10.1126/science.1165942 | |

Vanderweyde, T., Yu, H., Varnum, M., Liu-Yesucevitz, L., Citro, A., Ikezu, T., et al. (2012). Contrasting pathology of the stress granule proteins TIA-1 and G3BP in tauopathies. J. Neurosci. 32, 8270–8283. doi:10.1523/JNEUROSCI.1592-12.2012 | |

Veldink, J. H., Kalmijn, S., Van der Hout, A. H., Lemmink, H. H., Groeneveld, G. J., Lummen, C., Scheffer, H., Wokke, J. H., & Van den Berg, L. H. (2005). SMN genotypes producing less SMN protein increase susceptibility to and severity of sporadic ALS. Neurology, 65(6), 820–825.

Vietri, M., Schultz, S. W., Bellanger, A., Jones, C. M., Petersen, L. I., Raiborg, C., Skarpen, E., Pedurupillay, C. R. J., Kjos, I., Kip, E., Timmer, R., Jain, A., Collas, P., Knorr, R. L., Grellscheid, S. N., Kusumaatmaja, H., Brech, A., Micci, F., Stenmark, H., & Campsteijn, C. (2020). Unrestrained ESCRT-III drives micronuclear catastrophe and chromosome fragmentation. Nature cell biology, 22(7), 856–867.

Von Appen, A., LaJoie, D., Johnson, I. E., Trnka, M. J., Pick, S. M., Burlingame, A. L., Ullman, K. S., & Frost, A. (2020). LEM2 phase separation promotes ESCRT-mediated nuclear envelope reformation. Nature, 582(7810), 115–118. https://doi.org/10.1038/s41586-020-2232-x

Wang, I. F., Reddy, N. M., & Shen, C. K. (2002). Higher order arrangement of the eukaryotic nuclear bodies. Proceedings of the National Academy of Sciences of the United States of America, 99(21), 13583–13588.

Weber, G., Trowitzsch, S., Kastner, B., Lührmann, R., & Wahl, M. C. (2010). Functional organization of the Sm core in the crystal structure of human U1 snRNP. The EMBO journal, 29(24), 4172–4184.

Webster, B. M., Thaller, D. J., Jäger, J., Ochmann, S. E., Borah, S., & Lusk, C. P. (2016). Chm7 and Heh1 collaborate to link nuclear pore complex quality control with nuclear envelope sealing. The EMBO journal, 35(22), 2447–2467.

Webster, B. M., Colombi, P., Jäger, J., & Lusk, C. P. (2014). Surveillance of nuclear pore complex assembly by ESCIII/Vps4. Cell, 159(2), 388–401. https://doi.org/10.1016/j.cell.2014.09.012

Wegmann, S., Eftekharzadeh, B., Tepper, K., Zoltowska, K. M., Bennett, R. E., Dujardin, S., et al. (2018). Tau protein liquid-liquid phase separation can initiate tau aggregation. EMBO J. 37, e98049. doi:10.15252/embj.201798049 | |

Weis, K., and Hondele, M. (2022). The role of DEAD-box ATPases in gene expression and the regulation of RNA-protein condensates. Annu. Rev. Biochem. 91, 197–219. doi:10.1146/annurev-biochem-032620-105429 | |

Wheeler, J. R., Matheny, T., Jain, S., Abrisch, R., and Parker, R. (2016). Distinct stages in stress granule assembly and disassembly. Elife 5, e18413. doi:10.7554/eLife.18413 | |

Wheeler, E. C., Vu, A. Q., Einstein, J. M., DiSalvo, M., Ahmed, N., Van Nostrand, E. L., Shishkin, A. A., Jin, W., Allbritton, N. L., & Yeo, G. W. (2020). Pooled CRISPR screens with imaging on microRaft arrays reveals stress granule-regulatory factors. Nature methods, 17(6), 636–642.

Wijesekera, L.C., Nigel Leigh, P. Amyotrophic lateral sclerosis. Orphanet J Rare Dis 4, 3 (2009).
Will, C. L., & Lührmann, R. (2001). Spliceosomal UsnRNP biogenesis, structure and function. Current opinion in cell biology, 13(3), 290–301.

Wollny, D., Vernot, B., Wang, J., Hondele, M., Safrastyan, A., Aron, F., et al. (2022). Characterization of RNA content in individual phase-separated coacervate microdroplets. Nat. Commun. 13, 2626. doi:10.1038/s41467-022-30158-1 | |

Wolozin, B., and Ivanov, P. (2019). Stress granules and neurodegeneration. Nat. Rev. Neurosci. 20, 649–666. doi:10.1038/s41583-019-0222-5 | |

Xiong, X. P., Kurthkoti, K., Chang, K. Y., Lichinchi, G., De, N., Schneemann, A., MacRae, I. J., Rana, T. M., Perrimon, N., & Zhou, R. (2013). Core small nuclear ribonucleoprotein particle splicing factor SmD1 modulates RNA interference in Drosophila. Proceedings of the National Academy of Sciences of the United States of America, 110(41), 16520–16525.

Xu, C., Ishikawa, H., Izumikawa, K., Li, L., He, H., Nobe, Y., Yamauchi, Y., Shahjee, H. M., Wu, X. H., Yu, Y. T., Isobe, T., Takahashi, N., & Min, J. (2016). Structural insights into Gemin5-guided selection of pre-snRNAs for snRNP assembly. Genes & development, 30(21), 2376–2390.

Xu, F., Jia, M., Li, X., Tang, Y., Jiang, K., Bao, J., & Gu, Y. (2021). Exportin-4 coordinates nuclear shuttling of TOPLESS family transcription corepressors to regulate plant immunity. The Plant cell, 33(3), 697–713.

Xue, Y. C., Ng, C. S., Xiang, P., Liu, H., Zhang, K., Mohamud, Y., & Luo, H. (2020). Dysregulation of RNA-Binding Proteins in Amyotrophic Lateral Sclerosis. Frontiers in molecular neuroscience, 13, 78.

Yang, P., Mathieu, C., Kolaitis, R. M., Zhang, P., Messing, J., Yurtsever, U., et al. (2020). G3BP1 is a tunable switch that triggers phase separation to assemble stress granules. Cell 181, 325–345. doi:10.1016/j.cell.2020.03.046 | |

Yasuda, K., & Mili, S. (2016). Dysregulated axonal RNA translation in amyotrophic lateral sclerosis. Wiley interdisciplinary reviews. RNA, 7(5), 589–603.

Yi, H., Mu, L., Shen, C., Kong, X., Wang, Y., Hou, Y., & Zhang, R. (2020). Negative cooperativity between Gemin2 and RNA provides insights into RNA selection and the SMN complex's release in snRNP assembly. Nucleic acids research, 48(2), 895–911.

Yin, S., Lopez-Gonzalez, R., Kunz, R. C., Gangopadhyay, J., Borufka, C., Gygi, S. P., Gao, F. B., & Reed, R. (2017). Evidence that C9ORF72 Dipeptide Repeat Proteins Associate with U2 snRNP to Cause Mis-splicing in ALS/FTD Patients. Cell reports, 19(11), 2244–2256.

Yoshizawa, T., Ali, R., Jiou, J., Fung, H. Y. J., Burke, K. A., Kim, S. J., et al. (2018). Nuclear import receptor inhibits phase separation of FUS through binding to multiple sites. Cell 173, 693–705. doi:10.1016/j.cell.2018.03.003 | |

Youn, J. Y., Dunham, W. H., Hong, S. J., Knight, J. D. R., Bashkurov, M., Chen, G. I., et al. (2018). High-density proximity mapping reveals the subcellular organization of mRNA-associated granules and bodies. Mol. Cell 69, 517–532. e511. doi:10.1016/j.molcel.2017.12.020 | |

Zacco, E., Grana-Montes, R., Martin, S. R., De Groot, N. S., Alfano, C., Tartaglia, G. G., et al. (2019). RNA as a key factor in driving or preventing self-assembly of the TAR DNA-binding protein 43. J. Mol. Biol. 431, 1671–1688. doi:10.1016/j.jmb.2019.01.028 | |

Zhang, K., Donnelly, C. J., Haeusler, A. R., Grima, J. C., Machamer, J. B., Steinwald, P., Daley, E. L., Miller, S. J., Cunningham, K. M., Vidensky, S., Gupta, S., Thomas, M. A., Hong, I., Chiu, S. L., Huganir, R. L., Ostrow, L. W., Matunis, M. J., Wang, J., Sattler, R., Lloyd, T. E., … Rothstein, J. D. (2015). The C9orf72 repeat expansion disrupts nucleocytoplasmic transport. Nature, 525(7567), 56–61.

Zhang, K., Daigle, J. G., Cunningham, K. M., Coyne, A. N., Ruan, K., Grima, J. C., et al. (2018). Stress granule assembly disrupts nucleocytoplasmic transport. Cell 173, 958–971. doi:10.1016/j.cell.2018.03.025 | |

Zhang, P., Fan, B., Yang, P., Temirov, J., Messing, J., Kim, H. J., et al. (2019). Chronic optogenetic induction of stress granules is cytotoxic and reveals the evolution of ALS-FTD pathology. Elife 8, e39578. doi:10.7554/eLife.39578 | |

Zhang, K., Donnelly, C. J., Haeusler, A. R., Grima, J. C., Machamer, J. B., Steinwald, P., et al. (2015). The C9orf72 repeat expansion disrupts nucleocytoplasmic transport. Nature 525, 56–61. doi:10.1038/nature14973 | |

Zhou, Y., Zhou, B., Pache, L., Chang, M., Khodabakhshi, A. H., Tanaseichuk, O., Benner, C., & Chanda, S. K. (2019). Metascape provides a biologist-oriented resource for the analysis of systems-level datasets. Nature communications, 10(1), 1523. https://doi.org/10.1038/s41467-019-09234-6

Zhu, L., Xu, M., Yang, M., Yang, Y., Li, Y., Deng, J., et al. (2014). An ALS-mutant TDP-43 neurotoxic peptide adopts an anti-parallel beta-structure and induces TDP-43 redistribution. Hum. Mol. Genet. 23, 6863–6877. doi:10.1093/hmg/ddu409 | |

Zurla, C., Lifland, A. W., and Santangelo, P. J. (2011). Characterizing mRNA interactions with RNA granules during translation initiation inhibition. PLoS One 6, e19727. doi:10.1371/journal.pone.0019727 |